Enabling Efficient Sizing of Hybrid Power Plants: A Surrogate-Based Approach to Energy Management System Modeling

Charbel Assaad[1], Juan Pablo Murcia Leon[1], Julian Quick[1], Tuhfe Göçmen[1], Sami Ghazouani[2], and Kaushik Das[1]

[1]Department of Wind and Energy Systems, Technical University of Denmark, Roskilde, Denmark
[2]TotalEnergies, Paris, La Défense, France

Correspondence: Charbel Assaad (chass@dtu.dk)

Abstract.

~~Sizing~~ Optimal sizing of Hybrid Power Plants (HPPs), which include wind power plants and battery energy systems, is essential to ~~capture trade offs among various technology mixes. To accurately represent these trade-offs, an Energy Management System~~ prevent financial losses from under- or over-sizing relative to grid connection capacities. Accurate sizing requires high-fidelity Energy Management Systems (EMS) ~~is introduced to model the operation of a battery when participating in any market~~to model bidding strategies and operations in electricity markets, resulting in ~~realistic~~ precise operational revenues and costs. However, ~~traditional EMS models are computationally expensive to solve, a challenge that intensifies when integrating these modelsinto sizing processes. This research paper aims to address the critical~~ due to the computational burden of such models, sizing methodologies often resort to low-fidelity EMS models, leading to faulty sizing evaluations. To address the need for a computationally efficient ~~, accurate, and comprehensive operational~~ and accurate model that enables quantitative assessment of HPPs~~. A novel methodology is introduced~~ , we evaluate the potential of surrogate models to replace a high-fidelity EMS participating in the day-ahead electricity market in Denmark with perfect forecasts. Given the limited literature on surrogates of EMS models for utility-scale, grid-connected HPPs with batteries, we develop and compare four different surrogate models to approximate a state-of-the-art EMS model~~for HPPs involved in spot market power bidding. This approach utilizes~~ . The best-performing surrogate employs singular value decomposition for ~~dimension~~ dimensionality reduction and a feed-forward neural network ~~as a regression. The accuracy of our methodology is evaluated showing a~~ for regression. This surrogate achieves a normalized root mean square error of ~~0.09 in predicting hourly operational time series~~0.81% in approximating yearly revenues. This method proves effective in accurately evaluating the operation of HPPs across various geographical locations and hence ~~on~~ in multiple sizing problems. Furthermore, we ~~utilized~~ utilize the surrogate to evaluate the profitability of several ~~HPPs sizing~~HPP sizes, achieving a root mean square error of 0.010 on the profitability index~~. This shows~~ , with values ranging between -0.13 and 0.18. This demonstrates that the developed surrogate model is suitable for HPP sizing ~~for~~ under the given cost and financial assumptions.

1 Introduction

As the renewable energy and storage industry ~~has matured~~matures, governmental incentives ~~, that sustained~~ that sustain this rapid development ~~,~~ have started to shift. Initially sustained by government-supported feed-in tariffs, wind power ~~plant~~ plants are transitioning to feed-in premiums or ~~contracts for differences~~contracts-for-differences. As noted by Kitzing et al. (2024) , contracts-for-differences have become increasingly significant in the European market, particularly following an agreement reached in May 2024 between the European Commission, the European Parliament, and the Council (Council of the European Union, 2024) . This agreement mandates that the support for renewable technologies is provided through two-sided contracts-for-differences or equivalent schemes, applying to both new investments and repowering. These support levels are now determined through competitive bidding procedures ~~,~~ Busch et al. (2023). Additionally, the power plants are ~~also~~ expected to maximize their ~~values~~ value from energy markets such as the electricity spot market or balancing/reserve markets. This change exposes power plant developers to the dynamics of the wholesale electricity market. In this evolving landscape, ~~Battery Energy Storage Systems (BESS)~~ Hybrid Power Plants (HPPs) that include storage technology are becoming valuable ~~for wind power plants~~ to establish robust business cases.

Despite the absence of a universal definition for ~~Hybrid Power Plants (HPPs) -~~ HPPs — highlighted by varying interpretations in the literature (Dykes et al., 2020; Long et al., 2022; Paska et al., 2009) ~~–~~ — for the purposes of this research, we define renewable-based HPPs as power plants that combine several generation technologies, including wind turbines ~~,~~ and possibly energy storage, to produce electricity and other energy vectors. They operate from a single geographical location, with all generated power being transmitted to the electrical grid via a unified point of grid connection.

In the presence of a BESS, HPPs can use strategies such as market arbitrage, which involves buying and storing electricity when market prices are low and selling it when prices are high. Additionally, the integration of energy storage is crucial for smoothing power supply fluctuations, mitigating power curtailment, enabling HPPs to offer system services~~and reduce~~ , and reducing grid congestion (Das et al., 2019).

As HPPs transition to market-driven revenue models, ~~new possibilities and challenges emerge for power plant developers and operators. They can strategically navigate energy markets, tailor their operations to demand fluctuations, and capitalize on price differentials. Consequently, to optimally size an HPP and exploit its potential, it is crucial to consider detailed operational~~ optimizing their operations becomes essential to capitalize on market opportunities and address operational challenges. An EMS fulfills this role by devising optimal operational strategies throughout the power plant~~'~~'s lifetime. ~~This role is fulfilled by an Energy Management System (EMS). A comprehensive EMS takes into account the market structure in which the power plant operates, models the various technologies within the HPP , and aims to maximize profits through market biddings. The importance of a realistic EMS becomes more apparent when a HPP includes a storage system, as it is necessary to optimize the~~ For an HPP with a BESS, the EMS optimizes the charge and discharge power of the battery, given the available resources (i.e., wind speed, solar power), the battery's capacity, available grid connection capacity, and other constraints. In electricity trading, various markets allow power plant operators to sell their energy. The Spot Market (SM) is currently the most lucrative market where power is traded for immediate delivery. Within the SM, operators can participate in the day-ahead and ~~degradation~~

cost. Electricity markets often hour-ahead markets. Day-ahead bidding establishes hourly prices for the following day, while hour-ahead bidding allows for adjustments based on updated generation forecasts and cleared SM prices. Since electricity markets require power producers to bid in advance for the quantity on the amount of electricity they will generate and sell. These biddings are based on forecasting , these bids rely on forecasts of renewable energy generations as well as generation and market prices. However, when the If actual generation deviates from scheduled bids, financial penalties are incurred, accurate forecasting can mitigate these penalties . Hence, EMS operates . Additionally, the balancing market (BM) offers HPPs another revenue source, operating alongside the SM to handle discrepancies between forecasted and actual demand and supply. The BM allows transmission system operators to adjust for differences arising from SM bids that are based on earlier forecasts and the real-time conditions closer to delivery. This market acts in near real-time, addressing deviations from scheduled generation and imposing penalties as necessary. Consequently, an EMS aims to maximize profits , taking into account opportunities in by strategically storing and selling electricity , as well as in both the SM and BM, while also minimizing imbalance costs due to deviations from the scheduled energy bid. Consequently, numerous studies have approached EMS modeling as an optimization problem. For instance, Das et al. (2020b) established a problem formulation for a wind-battery power plant based on the scheduled energy bids.

In the field of hybrid renewable energy systems, particularly in microgrids, the dispatch problem has been extensively studied, as evidenced by numerous review articles on the topic (Barbosa et al., 2024; Shivarama Krishna and Sathish Kumar, 2015; Fathima . However, the primary purpose of microgrids is to manage or follow load profiles within a network, whereas HPPs operate as distinct generation facilities with a connection to the power grid. This unique connection emphasizes the role of HPPs in active power generation, rather than load management alone, which calls for a distinct EMS model such as the ones developed by Toubeau et al. (2021) and Ding et al. (2016).

EMS models vary in complexity and computational demand, and for this article, we categorize them into high-fidelity (HF) and low-fidelity (LF) models. High-fidelity EMS models provide detailed and accurate representations of HPPs, capturing intricate system dynamics, precise component behaviors, and sophisticated market interactions. These models incorporate forecasting and real-time data, comprehensive operational constraints, and optimize bidding strategies to maximize profits in electricity markets (Taha et al., 2018; Zhu et al., 2024; Ochoa et al., 2022; Han and Hug, 2020; Li and Qiu, 2016; Abdeltawab and Moham . While HF EMS models offer high accuracy in estimating operational performance and financial outcomes, they require significant computational resources and time. For instance, Huang et al. (2021b) develops a stochastic optimization-based HF EMS where solving the dispatch for one week of operation takes between 329 and 2,991 seconds, depending on the chosen optimization algorithm among five compared. Similarly, Li and Qiu (2016) present a deterministic HF EMS model that requires using a monthly time step to reduce simulation costs.

In contrast, LF EMS models simplify the representation of HPP operations by using aggregated system models, basic forecasting methods (or none), and simplified market participation strategies (An et al., 2020; Luo et al., 2015; Cai et al., 2016a; Zhang et a . They reduce computational demand by neglecting detailed component behaviors and operational constraints. Although they enable rapid simulations and are easier to integrate into optimization frameworks, their oversimplifications can lead to inaccuracies in revenue and cost estimations, potentially resulting in sub-optimal or erroneous sizing decisions. Table 1

provides an overview of the distinctions between HF and LF EMS models. Notably, there is no universally accepted standard for defining these classifications, so the table serves as a guideline based on key characteristics relevant to this study.

The trade-off between computational efficiency and model accuracy presents a significant challenge for the optimal sizing of HPPs. A sizing optimization of an HPP involves maximizing a financial metric by varying the wind power plant rating, battery energy, and power ratings. Calculating that financial metric requires solving an EMS model for each potential HPP configuration~~, resulting in considerable~~. Consequently, HF EMS models offer precise assessments; however, relying solely on them is impractical due to their substantial computational demands. ~~Indeed,~~ Conversely, using LF EMS models reduces computational time but risks compromising the financial viability of the ~~combination of generation and storage technologies introduce numerous time-dependent variables, complicating the optimization process for sizing an HPP. To illustrate this, we present a quantitative analysis of the required computational effort for optimal HPP sizing, based on an~~ project due to inaccurate assessments. To illustrate the computational burden of an HF EMS model, we evaluate the state-of-the-art EMS developed by Zhu et al. (2022). This model ~~will be further detailed in Section 2.1.~~

~~Table ?? illustrates why HPP~~ requires 1,250 minutes to solve for 25 years of operation (the assumed lifetime) of a given HPP using a single-node High Performance Computing (HPC) cluster, Sophia (DTU HPC Cluster, 2019), which has 32 physical cores (2 × sixteen-core AMD EPYC 7351) and 128 GB of RAM (4 GB per core, DDR4@2666 MHz). Therefore, even if we need to evaluate only a few sizings for the optimizer to converge, we require a substantial amount of time to reach a solution. For example, evaluating 10 sizings takes 12,500 minutes, or approximately 208 hours. Additionally, in previous work familiar to the authors (Leon et al., 2024), a sizing optimization can take up to several hundred iterations to approach optimality. In that study, the authors use a low-fidelity EMS model to evaluate the operation of an HPP over its lifetime in a matter of 15 seconds. The comparison of the optimization time is based on the same computational resources. Given these computational benefits, HPP sizing optimization often relies on ~~a simplified EMS representation. A complex EMS can extend the optimization process to thousands of hours, making a simplified EMS a common approach to reduce computational time. Although this approach may sacrifice some accuracy in predicted operational revenues, it is a common thread in numerous review studies (Roy et al., 2022; Lian et al., 2019; Thirunavukkarasu et al., 2023) that examine HPP sizing methodologies. These studies reveal a predominant preference for simplified operational strategies in the~~ LF EMS models. For example, Leon et al. (2024) propose a methodology for sizing HPPs as a nested optimization problem, using two LF EMS models: a short-term EMS formulated as linear programming and a long-term rule-based EMS. The short-term EMS provides a baseline for daily optimal operations, while the long-term EMS modifies these operations to account for degradation effects and forecast inaccuracies over the plant's lifetime. Similarly, in a study aimed at optimizing the design and layout of a hybrid wind-solar-storage plant, Stanley and King (2022) employs a simple battery dispatch model, where the battery is only discharged to meet minimum power requirements. While using LF EMS models may result in reduced accuracy in revenue estimation, they are widely adopted in HPP sizing ~~process. The methodologies are typically divided into deterministic and stochastic mathematical-based approaches, such as linear or dynamic programming models, which are well-suited for handling differentiable and continuous objective functions. While gradient-based numerical optimization has the advantage of guaranteeing local optimality, their applicability is limited to a subset of objective functions that are continuous and convex.~~ due to computational efficiency. Indeed, several review studies

underscore the prevalence of LF EMS models in sizing methodologies (Roy et al., 2022; Lian et al., 2019; Thirunavukkarasu et al., 2023) .

~~To evaluate the value of HPP, the Levelized Cost of Energy (LCoE) is traditionally used. However, to assess the various potential revenue streams, metrics such as Net Present Value (NPV) (Dykes et al., 2020) or the NPV over CAPEX (Capital Expenditure), are more relevant. This is because storage inherently increases costs and thus the LCoE, even though it has the potential to substantially increase revenue or profit.~~ It is challenging to quantify the accuracy loss when using LF EMS instead of HF models. Research studies often test EMS models on varied configurations of HPPs, and only a few conduct direct comparative analyses within the same setup, primarily focusing on high-fidelity EMS models. For instance, Ochoa et al. (2022) compare deep reinforcement learning with both stochastic optimization and robust optimization for photovoltaic-battery HPPs using U.S. market data, finding that deep reinforcement learning offers superior economic performance and significantly reduces computational time compared to the other two studied methods. Similarly, Han and Hug (2020) report that, in a one-year simulation using Nord Pool data, the distributionally robust optimization model achieves higher revenues than deterministic forecasting approaches. Zhu et al. (2024) further explore this by comparing EMS models that utilize distributionally robust optimization with those based on deterministic optimization and stochastic optimization for wind-battery hybrid plants in Nordic day-ahead markets, taking imbalance settlements into account. By adjusting the parameters of the distributionally robust optimization model, they demonstrate that the economic performance ranks highest for this approach, followed by risk-neutral stochastic optimization, and finally deterministic optimization. This approach enables more resilient offering strategies, especially in markets with high penalties for energy imbalances. Additionally, Zhu et al. (2024) examine the accuracy of total profits across three HF EMS models and show that even within these models, certain simplifications commonly found in low-fidelity models—such as the use of deterministic forecasts—can lead to revenue discrepancies of up to 7.6% compared to the best-performing model (refer to Table 3 of the referenced paper). Given these considerations, this paper primarily focuses on reducing the computational demand of high-fidelity EMS models.

~~Computational Effort for Optimal Sizing of an HPP using a complex EMS from Zhu et al. (2022) Time required for one sizing loop (sec) 10Iteration required to find refined solution 1,000 Time required to compute EMS output per HPP configuration (sec) 2,820 Total time to find the refined configuration (sec)28, 200,000~~ **~~Time in hours~~ ~~7,833~~**

To ~~overcome~~ address the computational challenges associated with implementing a realistic EMS for HPP sizing while maintaining high accuracy, a promising approach involves ~~the use of~~ using data-driven surrogate-based ~~optimization a technique that has shown promise in addressing~~ modeling. This technique demonstrates potential in tackling computationally intensive problems ~~in other domains .~~ across various domains (Zhang et al., 2021; Lin et al., 2023; Pang et al., 2023). These Reduced-Order Models (ROM) aim to replace high-dimensional, resource-intensive problems with models that are significantly faster to simulate while accurately representing the original solution behavior. In particular, Hesthaven et al. (2022) reviews the development of surrogates for time-dependent problems, including those with nonlinear dynamics, which are of interest in our work. In this context, data-driven surrogate models stand out as promising solutions, thanks to major advancements in machine learning methods. These models often follow an offline-online paradigm. During the offline phase, a reduced basis is extracted from a collection of high-fidelity solutions; this reduced basis is then used to train the surrogate model by optimizing weights or

coefficients that capture the system dynamics. Although this step is computationally intensive, it only needs to be performed once. In the online phase, the surrogate model uses the precomputed weights to compute new outputs almost instantly, with minimal computational cost. This paradigm enables the surrogate model not only to learn the mapping from inputs to outputs but also to understand underlying patterns within the input data, leading to faster and more accurate simulations. Numerous successful implementations of data-driven surrogate models exist in the literature. For instance, ~~Zhang et al. (2021) trained a deep reinforcement learning algorithm to derive the optimal control policy for the operation of~~ Hesthaven and Ubbiali (2018) develops an ROM using Proper Orthogonal Decomposition (POD) to extract a reduced basis from high-fidelity solutions and employs multi-layer perceptron neural networks to approximate the coefficients of the reduced model, although time-dependency is not considered. Similarly, Guo and Hesthaven (2019) uses a POD projection and maps the time and parameter values onto the reduced basis using tensor products of two Gaussian processes—one for time and one for parameters. Hess et al. (2023) utilizes a ~~small-scale wind-solar-diesel-battery-reverse osmosis energy system. In a similar approach, ? developed a Kriging-based surrogate model to substitute the computationally expensive objective functions. Consequently, the combined economic and emission dispatch problem in large-scale power systems was efficiently solved with suitable accuracy. Furthermore, Pang et al. (2023) employed a neural network surrogate model to replace the original fuel cost functions, reducing the execution time . This neural network was integrated with a~~ data-driven ~~bat algorithm that efficiently addressed the economic dispatch problemwithin a comparatively shorter timeframe than other tested approaches. Despite the advancements in surrogate modeling for various applications, there remains a gap for surrogate~~ ROM approach to efficiently compute the Rayleigh–Bénard cavity problem, integrating POD, dynamic mode decomposition, and manifold interpolation for a robust and computationally efficient model. Departing from POD, Bhatt et al. (2023) employs deep auto-encoder networks to compress high-fidelity snapshots before using these in forecasting models—specifically, long short-term memory and temporal convolutional networks for time-series forecasts, and convolutional neural networks for spatial feature extraction—significantly reducing computational costs in both the offline and online stages. Most ROMs have been applied to problems described by partial differential equations with sharp gradients. In contrast, our aim is to apply similar techniques to high-fidelity EMS models for HPPs. Although surrogate modeling has advanced across multiple fields, a gap remains in developing models tailored to EMS for utility-scale HPPs~~incorporating~~ , particularly those that incorporate detailed operational strategies for market participation. This gap exists not only due to the ~~lack~~ scarcity of existing applications of surrogate models for EMS in HPPs but also because of the complexity involved in designing an accurate surrogate model based on a multitude of input and output time series. ~~Utility-scale HPPs require precise and reliable predictions to optimize performance and profitability, and the variability in market conditions and operational constraints further complicates the creation of effective surrogate models. Additionally,~~ Additionally, integrating the surrogate model ~~needs to be integrated~~ within a sizing evaluation framework adds another layer of complexity.

This article seeks to ~~address the critical need for a computationally efficient, accurate, and comprehensive operational model that enables quantitative~~ evaluate the potential of data-driven surrogate models in reducing the computational burden of high-fidelity EMS models, while preserving the high accuracy needed for a reliable assessment of HPPs. ~~For that,~~ To achieve this, we develop four surrogate models ~~are used~~ to approximate the outputs of the ~~high-fidelity EMS. Two of which use a~~ HF EMS. We begin by employing two models based on multivariate linear regression~~to establish a baseline and two others~~

~~are~~ , which serve as baselines due to their simplicity, interpretability, and low computational cost. Recognizing that the EMS exhibits complex and nonlinear behaviors that linear models may not capture adequately, we also develop two models based on Neural ~~networks~~ Networks (NNs). ~~Thanks to the variety of the NN's activation functions, the inherent non-linear behavior of the high-fidelity EMScan be approximated. This paper builds on top the EMS~~ Neural networks, particularly Feed-forward Neural Networks (FNNs), are capable of modeling intricate nonlinear relationships through their layered architectures and nonlinear activation functions. This makes them well-suited for approximating the inherent nonlinear dynamics of the HF EMS. By leveraging NNs, we can capture complex patterns and interactions within the data that linear models might overlook, potentially achieving higher accuracy in estimating outputs. The choice of these surrogate models allows us to explore the trade-offs between model complexity, computational efficiency, and accuracy. By comparing the performance of multivariate linear regression models and neural networks, we assess the extent to which incorporating nonlinearity improves the surrogate's ability to replicate the HF EMS outputs. Additionally, NNs have demonstrated success in surrogate modeling across various fields due to their flexibility and scalability, making them a promising candidate for this application.

Building upon the EMS model developed by Zhu et al. (2022), which ~~will be~~ is detailed in the following section~~.~~ , this paper seeks to answer the question: How can we enable the sizing evaluation of utility-scale HPPs based on an accurate and computationally efficient EMS model?

The major contributions of this article are as follows:

- Development of a fast and ~~precise surrogate~~ accurate surrogate model for a utility-scale HPP EMS ~~model~~ participating in the spot market. ~~The surrogate is based on a Feed-Forward Neural Network (FNN), harnessing the power of machine learning to provide a reliable and efficient alternative to the computationally intensive EMS model.~~
- ~~Assessment~~ Demonstration of the surrogate's ~~ability to predict hourly operational time series on multiple sites across~~ generalizability in different geographical locations within the same electricity market region.
- Integration of the developed surrogate within a ~~framework to evaluate~~ sizing evaluation framework to accurately assess the profitability of ~~an HPP sizing with high accuracy~~various HPP configurations.

The remainder of this paper is organized as follows~~. Section 2 introduces the~~ : Section 2 the HF EMS model that the ~~surrogate is based on ,~~ surrogates are based on and the methodology devised for the surrogate modeling of the EMS~~, and~~ . Section 3 details the sizing evaluation framework for analyzing the profitability of an HPP using the HF EMS and the surrogate models. Section 4 provides details on the case study, the data used to train and validate the surrogate ~~as well as the cost model for the sizing evaluation framework. While Section 5 provides~~ models, while Section 5 offers an in-depth analysis of the ~~surrogate's accuracy~~ best-performing surrogate and its application. The performance of all surrogates is detailed in Appendix A. These results are put into perspective in Section 6 and summarized in Section 7.

2 Methodology

In this section, we ~~will start~~ begin by presenting the high-fidelity model that serves as the foundation for the surrogate models ~~,~~ in Section 2.1, followed by the methodology for developing the ~~surrogate model~~ four surrogate models in Section 2.2.

2.1 HPP Operation Model (EMS)

The EMS model, on which the surrogate is built, is presented in this section. The EMS model is based on a study by Zhu et al. (2022) that ~~focused~~ focuses on a co-located wind-battery HPP. This novel EMS model ~~, was~~ is formulated to optimize market participation within two sequential electricity markets: ~~namely, the spot market (SM) and the Balancing Market (BM), which encompasses~~ the SM and the BM, which encompass the regulatory periods of the Danish market structure. This ~~state of the art~~ state-of-the-art EMS has the advantage of considering ~~:~~

- Long-term operation of the HPP with comprehensive revenue ~~streams~~ stream calculations.
- Grid capacity ~~,~~ as a practical constraint for the HPP.
- ~~Possibility~~ The possibility of considering overplanting, which has been shown to increase the value of ~~HPP~~HPPs.

~~In electricity trading, various markets enable power plant operators to sell their energy. The SM is currently the most lucrative market where power is traded for immediate delivery. In the SM, power plant operators can bid on the day-ahead and hour-ahead markets. Day-ahead bidding determines hourly prices for the next day, while hour-ahead biddings allows for adjustments based on updated generation forecasts and cleared SM prices. The BM, another potential source of revenues for HPPs, operates in conjunction with the Spot Market (SM). The BM enables transmission system operators to adjust for discrepancies between forecasted and actual demand and supply. These discrepancies arise from the predicted electricity supply that were forecasted during the SM bidding process and the actual conditions closer to the delivery time. Hence, the BM acts in near real-time, penalizing deviations from scheduled generation. This~~ However, this paper primarily focuses on the EMS's role in ~~Day-Ahead (DA)~~ day-ahead SM participation. Additionally, our study considers the Danish market structure with a dispatch interval of 15 minutes. As in real power plants, the ~~EMS~~ SM bidding process (also referred to as SM optimization) communicates with a ~~Power Management System (PMS)~~ Real-Time (RT) dispatch optimization. In this framework, the ~~EMS~~ SM optimization provides energy set-points ~~,~~ based on weather and market forecast data to the ~~PMS~~RT dispatch, which, in turn~~uses Real-Time (RT) ,~~ uses real-time measurement data to derive ~~RT~~ real-time power values. ~~RT~~ Real-time measurements allow the calculation of deviations and the ~~applications~~ application of penalties. The ~~PMS is emulated as an active power control logic, as described in Long et al. (2022). The~~ inputs to the ~~EMS~~ SM optimization are time series forecasts of wind power and market prices, while the ~~PMS use~~ RT dispatch uses the same input time series updated ~~to RT measurements ,~~ with real-time measurements for each dispatch interval, as well as the bidding schedule generated from the ~~EMS~~SM optimization. For clarity, the inputs and outputs of the ~~EMS and PMS~~ SM optimization and RT dispatch are listed in Table 2. The combined models, SM optimization and RT dispatch, are referred to as a high-fidelity EMS model in this paper.

While the ~~EMS's inputs~~ SM optimization's input and output time series are based on hourly time steps, the ~~PMS~~RT dispatch's outputs and ~~RT~~ real-time input time series have a time step equal to the dispatch interval, i.e., 15 ~~min for the the~~ minutes

for the Danish market structure. Additionally, both models assume a given HPP configuration, also ~~denoted~~ referred to as sizing parameters in this article. ~~They~~ These are defined as the wind power plant rated power (P^W), the rated battery power ~~rating~~(B^P), battery energy capacity ~~rating~~(B^E), and grid connection power capacity (P^G). Other battery parameters~~such as the~~ , such as charge/discharge efficiency, are assumed from Zhu et al. (2022).

Figure 1 illustrates the considered EMS workflow. ~~EMS for Spot Market workflow. Adapted from Zhu et al. (2022)~~

~~The EMS itself is~~ The EMS operates through a structured daily cycle, beginning with the forecasting stage. On the previous day (d-1), a forecast of wind generation and spot market prices for the following day (d) is obtained. Using this data, the SM optimization is conducted at noon on day d-1, aligning with the day-ahead market closure, to determine the optimal hourly power bidding for the HPP. This optimization is formulated as a Mixed Integer Linear Programming (MILP) ~~model, executed once daily, at the beginning of each day. It aims at maximizing the revenues throughout the time span of the inputs. The PMS takes the form of~~ problem, aiming to maximize the plant's revenue across the day by strategically bidding power on the SM. On day d, the RT dispatch optimization is executed at 15-minute intervals throughout the day. This phase focuses on minimizing discrepancies between the power that was bid on the spot market and the actual real-time available power. The RT dispatch is modeled as a Mixed Integer Quadratic Programming (MIQP) ~~model, executed at regular dispatch intervals. The PMS minimizes the difference between the power bidding on the SM and the real-time available power~~problem, which dynamically adjusts the HPP's output to meet market commitments as closely as possible, responding to variations in generation. Finally, the day concludes with a settlement process on day d+1, where the outcomes of the day's operations are reconciled. The details of ~~both~~ all models can be found in the referenced work.

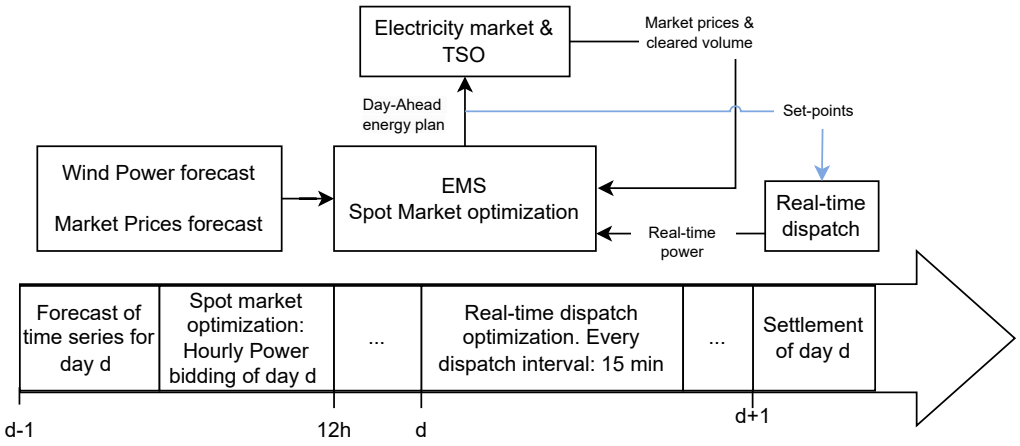

Figure 1. Workflow of HF EMS of this article, developed by Zhu et al. (2022)

The optimization models were solved using the solver of IBM Decision ~~Optimisation~~ Optimization Studio CPLEX through the docplex ~~python library (IBM, 2023)operating on the~~ Python library (IBM, 2023), operating on DTU's high-performance computing cluster~~Sophia (?).~~

, Sophia (DTU HPC Cluster, 2019). It was observed that for a given HPP configuration, 47 minutes were required to compute the outputs for one year of operation of the HF EMS model. The underlying reason for this is due to the iterative and sequential nature of the framework. For each day, the MILP optimization is solved first, followed by the MIQP for each dispatch interval (e.g., 96 times ~~a~~ per day). While each iteration of the MILP and MIQP problems requires a minimal amount of time (less than 0.15 seconds), the frequency of these optimizations is substantial. Moreover, since each time step depends on the previous one, it is necessary to perform the optimization sequentially. Table 3 shows the number of decision variables and constraints required to optimize for inputs spanning over one year. This highlights the substantial computational time ~~that would be~~ required to optimize the sizing of ~~a~~ an HPP based on such an operational model.

While the combination of both models allows for a realistic representation of the operation of ~~a~~ an HPP, it has its own limitations. These limitations are also carried over to the surrogate that is ~~build~~ built upon both models. No battery degradation model is considered in the optimization process. It is well known that lithium-ion batteries' energy capacity ~~degrade~~ degrades over time in a ~~non-linear~~ nonlinear fashion (Xu et al., 2018), ~~this~~ which directly impacts revenues as opportunities for energy arbitrage are reduced. Additionally, as we ~~are focusing~~ focus on demonstrating the potential of surrogate modeling for EMS of ~~HPP~~HPPs, perfect forecast data will be used. Finally, the balancing market will not be considered in this article and will be left ~~as a future works. The combined models, EMS and PMS, are referred to as a high-fidelity EMS model in this paper.~~ for future work.

2.2 Surrogate Methodology

In this article, a surrogate model consists of several sub-components: data pre-processing, a regressor, and data post-processing. The pre-processing ~~consists of scalingthat ensures~~ involves scaling, which ensures that all inputs contribute equally to the model's ~~predictions and helps~~ estimations and supports the surrogate's convergence algorithm. The post-processing is applied in accordance with the pre-processing to interpret the results in their original scale. The regressor is the model tasked with approximating the high-fidelity EMS. Section 2.2.1 details the inputs and outputs for training and evaluating the surrogate models. Section 2.2.2 describes four surrogate models, differing in their data processing and regressor ~~model~~models. Sections 2.2.3 and 2.2.4 cover the training and validation of these models, respectively.

2.2.1 Surrogate Model's Inputs and Outputs

Regardless of the surrogate model being evaluated, all models aim to approximate the same output time series given the same input data. Table 4 below lists the various input and output time series used to train and validate the surrogate.

The input time series of the surrogate match those of the ~~EMS~~SM optimization, and its outputs align with the ~~PMS~~RT dispatch's outputs. In addition to the input time series, the regressor also considers three scalar parameters representing an HPP, which ~~helps~~ help differentiate between various HPP configurations. ~~They~~ These parameters are represented by ~~equations 1 to ??:~~

P^W/P^G

B^P/P^G

B^E/B^P

Where P^W is the rated power of the wind power plant, P^G is the grid connection capacity, B^P is the rated battery power, and B^E is the rated energy capacity of the batterythe ratios P^W/P^G, B^P/P^G, and B^E/B^P.

2.2.2 Surrogate Models

Table 5 presents all surrogate models evaluated. Surrogate models tested **Pre-processing** **Regressor** **Post-processing** Normalization Linear Reverse Normalization Normalization Reverse SVD SVD Reverse Normalization Normalization FNN Reverse Normalization Normalization Reverse SVD SVD Reverse Normalization

The first surrogate, S1, which serves as our benchmark, normalizes the input and output time series for each HPP configuration and employs a multivariate linear regression to predict compute the normalized outputs from normalized inputs. Details on the normalization process appear later on, in this section.

The second surrogate, S2, incorporates a dimensionality reduction method known as Singular Value Decomposition (SVD), as developed by Gene H. Golub (1996). After normalizing inputs and outputs, we apply SVD, a common tool in numerical analysis, particularly for dimensionality reduction. The specific use of this method is detailed in this section.

The third and fourth surrogate models Surrogate models S3 and S4 are similar to the first and second onesS1 and S2, but they differ in their choice of regressors. Instead of employing a multivariate linear model, these models utilize a tuned FNN to capture the non-linear relationships between inputs and outputs.

For all surrogate models, we apply data post-processing consistent with the pre-processing to ensure the output data is interpretable in its original scale.

For all surrogate models, we normalize the wind power generation time series (W_t) using the turbine's rated power ,and the spot market price time series (SM_t) by the maximum price, achieving a scaling between zero and one. Since the output time series magnitudes depend on the sizing inputs, we use these parameters as the basis for normalization . This step refers to the Normalization in Table 5. It is applied for each time series following these equations:

$$P_{t,norm}^{sm,HPP} = P_t^{sm,HPP}/P^G \tag{1}$$

$$P_{t,norm}^{sm,dis,dis} = P_t^{sm,dis,dis}/B^P \tag{2}$$

$$P_{t,norm}^{sm,cha,cha} = P_t^{sm,cha,cha}/B^P \tag{3}$$

$$P_{t,norm}^{sm,curt,curt} = P_t^{sm,curt,curt}/(P^W - P^G) \tag{4}$$

~~In Equation (1) the power bidding on the SM is normalized by the grid capacity. Equations (2) and (3) normalized the battery charge and discharge profiles by the battery's rated capacity, and Equation (4) normalized the curtailed power with respect to the difference between wind power and grid capacity. A surrogate model, using only normalization for data processing, has five input features: SM_t, W_t, P^W/P^G, B^P/P^G, and B^E/B^P. It outputs four features: P_t^{sm}, $P_t^{sm,dis}$, $P_t^{sm,cha}$, and $P_t^{sm,curt}$.~~

~~We apply SVD method,~~ We apply the SVD as described in Zhu et al. (2010) ~~,~~ to derive the principal component matrices~~, denoted as Z in the cited paper~~. This method is used independently for the matrices containing the input time series M_{in} and the output time series M_{out}. The SVD is ~~used~~ applied following the normalization described above and ~~it is applied for the 2^{nd}~~ is used for surrogate models S2 and ~~4^{th} surrogate models of Table 5~~S4. Figure 2 illustrates the matrix M_{in}, which includes all normalized input time series for a single HPP configuration~~. Matrix M containing input time series, denoted M_{in}~~

~~In this figure, the notation $W_{t,norm,d}^{HPP_n}$ refers to the~~ : the normalized wind power time series for day d and for the HPP configuration n~~. Similarly, $SM_{t,norm,d}^{HPP_n}$ refers to~~ , $W_{t,norm,d}^{HPP_n}$, and the normalized SM prices ~~for day d for the HPP configuration n.~~ $SM_{t,norm,d}^{HPP_n}$.

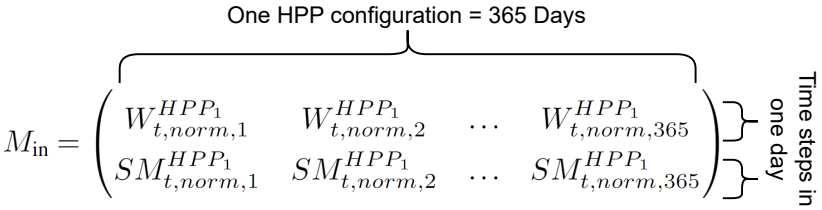

Figure 2. Matrix M containing input time series, denoted M_{in}. $W_{t,norm,d}^{HPP_n}$ is the normalized wind power time series for day d and for the HPP configuration n. $SM_{t,norm,d}^{HPP_n}$ is the normalized SM prices

As the high-fidelity EMS uses hourly time steps for forecasted wind power and SM prices, each of the input ~~vector~~vectors, $SM_{t,norm,d}^{HPP_n}$ and $W_{t,norm,d}^{HPP_n}$, ~~is of shape $(24,1)$. Hence, for a given HPP configuration, matrix M_{in} from Figure 2 is of shape $(24 \cdot 2, 365)$.~~ has 24 time steps. To expand this matrix for all HPP configurations, we concatenate horizontally (i.e., along the second dimension) each matrix M_{in} corresponding to ~~a~~ an HPP configuration. ~~We thus obtain a matrix of shape $((24 \cdot 2) \cdot N, 365)$. Where N is the number of HPP configurations.~~

The output time series matrix, M_{out}, is constructed in a similar fashion. However, unlike M_{in}, this matrix contains ~~fours~~ four time series, the ones defined in ~~equation~~ Eq. (1) to (4). ~~Additionally,~~ Note that these time series have a time step equal to the dispatch interval, e.g., 15 ~~min. Thus, M_{out} will be of shape $((96 \cdot 4) \cdot N, 365)$.~~ minutes.

After applying Singular Value Decomposition (SVD) to both matrices, M_{in} and M_{out}, we extract their principal component matrices ~~, Z_{in} and Z_{out}, and~~ and truncate them to the desired level. As a result, we obtain two sets of matrices with different truncation levels, denoted as r_{in} and r_{out}~~respectively. We use these truncated matrices for training and evaluating the regressor models.~~

, respectively. The truncation level is chosen so that the explained variance is 99%; for the definition, see Eq. 4 of Freire and Ulrych (1988). Table 6 presents an overview of the features and samples of each data-processing method for input and output data spanning over a year.

From this table, we observe that the features of the SVD method are ~~most~~ likely higher than ~~than the one~~ those derived from the normalization method (this depends on the truncation level). However, the number of samples ~~are~~ is substantially lower, ~~this~~ which allows us to achieve a reduced representation of the data. Note that the surrogate models using only normalization for data processing (S1 and S3) have five input features:: SM_t, W_t, P^W/P^G, B^P/P^G, and B^E/B^P. And they output four features: P_t^{HPP}, P_t^{dis}, P_t^{cha}, and P_t^{curt}.

2.2.3 Surrogate Training

To train a surrogate model, a training dataset is defined based on a number of HPP configurations with distinct sizing parameters. The details of this dataset can be found in Section 4. More specifically, this training dataset is used to train the SVD transformation and the two regressor models. Note that ~~the~~ normalization does not require ~~a~~ training. Two models are used to approximate the outputs of the high-fidelity EMS: a tuned FNN ~~and~~ (models S3 and S4) and a multivariate linear regression (models S1 and S2). The latter is used as a baseline model to compare the accuracy of the neural networks.

~~The training of FNN with hidden layers~~ Since the regressors used in S1 and S2 differ significantly from those in S3 and S4, their training processes also vary. Models S3 and S4 use an FNN; hence, the training is done in two steps ~~. Initially,~~ and applied for each of models S3 and S4 individually. The first step involves a tuning process and is carried out using two hyperparameters, shown in Table 7 below. ~~Afterwards, the best-performing model from the tuning process is selected for a more exhaustive training.~~

~~FNN grid search hyperparameter space **Hyperparameter Range Step** Layers 3,91 Neurons per layer 40,8020~~

Within this tuning process, it's important to note that each layer can have a varying number of neurons within the provided range. ~~A Rectified Linear Unit (ReLu) activation function has been used for all hidden layers and , for the output layer, a linear activation function has been used. ReLu is an appropriate activation function for the data, particularly following the normalization process, as all input and output time series become non-negative.~~

Afterwards, the best-performing model from the tuning process, for each of S3 and S4, is selected for more exhaustive training. This two-step approach is necessary to reduce the computational burden introduced by the tuning process, in which several hundred NN architectures are evaluated; however, the NNs aren't trained until they converge. Instead, the best-performing model from the tuning process is selected for further training. To efficiently select the hyperparameters among the search space, Hyperband by Li et al. (2018) ~~,~~ is used. Hyperband uses random sampling of hyperparameters to explore a wide range of settings.

~~A NN is defined by its architecture, parameters, and hyperparameters. The architecture consists of layers, starting with the input layer whose neuron count is determined by the dimensionality of the input data. This layer is followed by several hidden layerswith a given number of neurons and activation functions. These layers and neurons defines the network's depth and width, while the activation functions can introduce non-linearity into the model. The output layer has as many neurons as the~~

~~variables in the output data. The interconnections between these layers defines the topology of the NN. The parameters of the NN are the learnable weights and biases, which are determined in the training process. In contrast, the hyperparameters are pre-defined settings that are not learned from the training data. These encompasses the number of hidden layers, neurons per layer and much more~~For both models S3 and S4, a Rectified Linear Unit (ReLU) activation function is used for all hidden layers, and for the output layer, a linear activation function is used. ReLU is an appropriate activation function for the data, particularly following the normalization process, as all input and output time series become non-negative. To train ~~a~~ an NN, at least ~~2~~ two settings need to be defined. First, a loss function, which ~~is a metric that measure~~ measures the error between the training data and the model's ~~prediction - estimations~~—the mean squared error ~~was~~ is used. Second, an optimizer, which modifies the model's weights and biases during the training process to minimize the loss function. Each optimizer has its own set of hyperparameters. The Adam optimizer by Kingma and Ba (2017) ~~was~~ is used with a learning rate of 10^{-4}

~~The tuning process aims to evaluate several thousands of NN architectures. To avoid a computationally expensive process, these NN aren't trained until they converge. Instead, the best-performing model, from the tuning process, is selected for further training.~~

~~The tuning resulted~~ . The tuning results in the architectures presented in Table B1 and B2 in AppendixB.

~~The multi-variate linear regression is~~ Models S1 and S2 use multivariate linear regression. They are trained using the same dataset with the objective of minimizing the mean squared error, using the same optimizer as for the FNN.

Models S1 and S2 are not subject to any tuning, as there are no hidden layers or neurons. Similarly, the ~~SVD~~ ~~transformations were~~ SVD transformations are trained on the training dataset. The transformations ~~were~~ are trained separately for both input and output time series, resulting in two distinct transformations. ~~The normalization requires no training.~~

2.2.4 Surrogate Validation

We aim to identify the surrogate model ~~offering~~ that offers the best compromise between training time, inference time, and accuracy. First, we assess each surrogate's accuracy on a validation dataset, which is separate from but defined similarly to the training dataset. We measure the accuracy of each surrogate using the Root Mean Square Error (RMSE) between the ~~predicted and actual~~ estimated ($\hat{y}_{i,norm}$) and actual ($y_{i,norm}$) values for the normalized hourly time series and for all data points in the validation dataset (N). The RMSE (ϵ_{RMS}) is computed as follows:

$$RMSE\epsilon_{RMS} = \sqrt{\frac{1}{N}\sum_{i=1}^{N}(y_i - \hat{y}_i)^2}\sqrt{\frac{1}{N}\sum_{i=1}^{N}(y_{i,norm} - \hat{y}_{i,norm})^2} \tag{5}$$

~~Where:~~

y_i is the true data, within the validation dataset

$\hat{y}_i$ is the predicted data, based on validation dataset inputs

N is the number of data points

Since this RMSE ~~takes into account all the~~ is calculated across all output time series, it provides a ~~holistic measure~~ broad assessment of the model's accuracy, without specific insights into each individual series. We use this metric to compare the performance of the surrogate models presented in Table 5. Additionally, we measure the training ~~an~~ and inference time of each model.

For the best-performing surrogate model, among S1-S4, we further investigate the accuracy of each output time series using RMSE for a deeper understanding of the model. Our focus then shifts to one specific output time series, the normalized power output ~~$P^{sm}_{t,norm}$~~ $P^{HPP}_{t,norm}$. This time series allows us to calculate the yearly revenues, which are required to compute the Profitability Index (PI), ~~the~~ enabling us to evaluate the profitability of a given sizing, the key application of our surrogate in this article.

To explore the methodology's potential further, we assess the surrogate's generalizability across various locations within the western Danish price region, DK1. ~~For~~ In this intra-generalizability analysis, we calculate the Normalized ~~RMSE~~ Root Mean Square Error (NRMSE) of ~~yearly revenues, defined as follows:~~

the yearly revenues to assess the accuracy of the surrogate's approximations. Specifically, we compare the approximated revenues ($\hat{\Pi}_k$) with the actual revenues from the HF EMS (Π_k) for each HPP configuration k across all configurations in the selected set K. To express the RMSE as a relative measure, we normalize it by dividing by the median of the yearly revenues for all selected HPP configurations ($Median(\Pi)$), as computed by the HF EMS. The NRMSE (ϵ_{NRMS}) is given as:

$$NRMSE \epsilon_{NRMS} = \frac{\sqrt{\frac{1}{K}\sum_{k=1}^{K}(\Pi_k - \hat{\Pi}_k)^2}}{Median(\Pi)} \tag{6}$$

~~Where:~~

K is the number of HPP configurations.
in the validation dataset.

Π_k is the revenue of the k^{th} HPP configuration,
based on true data.

$\hat{\Pi}_k$ is the revenue of the k^{th} HPP configuration,
based on predicted data.

Median(Π) is the median revenue of all HPP
configurations, based on true data.

~~The revenues~~ The revenue time series is extracted from either true/observed data (from the high-fidelity model) or ~~predicted~~ approximated (from the surrogate model) power time series~~as follows:~~

$$\Pi = \sum_{i=t}^{T} P_t^{sm} \cdot \lambda_t^{sp} \cdot \Delta t$$

~~Where Π is the yearly revenue, Δt the time step, and T ~~, considering the dispatch interval Δt and the total time steps within a year~~.~~ T.

$$\Pi = \sum_{i=t}^{T} P_t^{HPP} \cdot SM_t \cdot \Delta t \tag{7}$$

3 Application: PI Evaluation

To assess the business case of ~~a~~ an HPP, we can use financial metrics like Internal Rate of Return (IRR) and Net Present Value (NPV). IRR calculates the HPP's annual investment return, while NPV assesses its profitability in today's value. However, when an HPP isn't profitable, resulting in a negative NPV, the IRR becomes undetermined. A more meaningful measure is the Profitability Index (PI), calculated as ~~NPV divided by the initial investment (CAPEX)~~$NPV/CAPEX$. The PI indicates how many dollars of present value benefit are generated per dollar of investment, offering a more intuitive understanding of the investment's profitability. This metric allows for a direct comparison of the relative profitability of each project, regardless of their absolute size. Additionally, when resources are limited, ~~NPV/CAPEX~~ $NPV/CAPEX$ can aid in prioritizing projects. Projects with higher PIs can be prioritized as they promise greater returns per unit of investment. A PI greater than 1 signifies that the NPV of future cash flows exceeds the initial investment. Note that traditionally, for power plants using one type of generation technology, the Levelized Cost of Energy (LCoE) is used to evaluate profitability. However, to assess the various potential revenue streams, metrics such as NPV (Dykes et al., 2020) or the NPV/CAPEX are more relevant. This is because storage inherently increases costs and thus the LCoE, even though it has the potential to substantially increase revenue or profit.

To compute the PI, we require the NPV, which in turn requires accurate yearly revenues and costs over the HPP's lifetime, aligning with the ideal framework shown in ~~Figure 3a~~Fig. 3(a). Yet, as discussed in the Introduction and Section 2.1, this method is computationally demanding. We instead use an alternative framework in ~~Figure 3b~~Fig. 3(b), utilizing the developed surrogate. This surrogate replaces the high-fidelity EMS, significantly reducing computational time and making the framework's execution feasible. The accuracy of this framework, employing the surrogate model to evaluate the PI, is presented in Section 5.4.

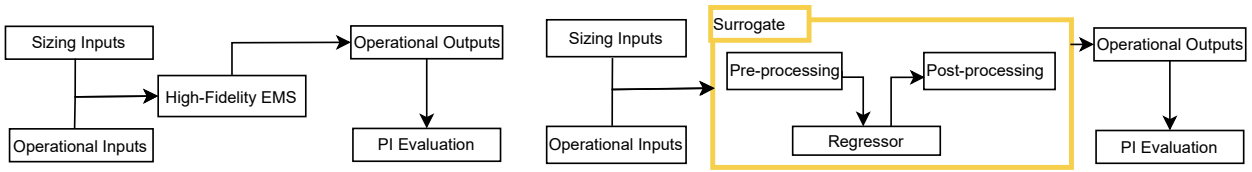

Figure 3. High-level sizing framework. Left: Ideal sizing evaluation framework using the High-Fidelity EMS. Right: Developed sizing evaluation framework using a surrogate of the EMS.

The PI varies between each sizing configuration (denoted as x), represented by P^G, P^W, B^E, B^P. PI is calculated as follows:

$$PI = \frac{NPV(x)}{CAPEX(x)} \tag{8}$$

~~Where:~~

$x = [P^G, P^W, B^E, B^P]$

The financial model is based on the yearly ~~cashflow~~ cash flow (CF_y) and the discount rate after tax (r_{AT})~~as defined below:~~ throughout the lifetime of the power plant Y.

$$NPV = \sum_{y}^{Y} \frac{CF_y}{(1 + r_{AT})^y}$$

Where Y is the lifetime of the power plant. The ~~cashflow~~ cash flow is calculated based on yearly profits (~~$Profit_y$~~ P_y) and CAPEX.

$$CF_y = \begin{cases} P_y & \text{for } y > 0 \\ -CAPEX & \text{for } y = 0 \end{cases}$$

It is important to highlight that the yearly profits are based on the revenues from the surrogate or the high-fidelity EMS (Π_y), as well as, the Operational Expenditure ($OPEX_y$), the tax rate (τ_{tax}), and the r_{AT}.

$Profit P_y = (\Pi_y - OPEX_y) \cdot (1 - \tau_{tax})$

The cost model used to calculated the $CAPEX$ and $OPEX$ is ~~define below:~~

$$\begin{aligned}
CAPEX &= C_w + C_b + C_{el} \\
OPEX_y &= O_{w,y} + O_{b,y} + O_{el,y} \\
C_w &= (WT_{cost} + WT_{civil}) \cdot P^W \\
C_b &= Nb_{eq} \cdot B^E_{cost} \cdot B^E + (B^P_{cost} + B^P_{civil} + B^P_{control}) \cdot B^P \\
C_{el} &= (HPP_{BOS} + P^G_{cost}) \cdot P^G + Land_rent \\
O_{w,y} &= WT^{OM}_{fixed,y} \cdot P^W + mean(AEP) \cdot WT^{OM}_{variable,y} \\
O_{b,y} &= B^{E,OM}_y \cdot B^E \\
O_{el,y} &= 0
\end{aligned}$$

~~Where C_w, C_b, C_{el} are the CAPEX of the wind power plant, batteries and the balance of system. Similarly $O_{w,y}$, $O_{b,y}$, and $O_{el,y}$ are the yearly OPEX from the wind power plant, batteries, and balance of system. The WT_{cost} and WT_{civil} are the wind turbine's cost and civil works in $Euro/MW$. Nb_{eq} is the number of battery equivalent in today's value. We will elaborate on~~

this metric shortly. B^E_{cost} is the battery energy cost per MWh while B^P_{cost}, B^P_{civil}, $B^P_{control}$ are the battery power cost, civil costs and control system costs per MW. HPP_{BOS} and P^G_{cost} are the shared Balance Of System (BOS) cost and grid connection cost of the HPP. $WT^{OM}_{fixed,y}$ and $WT^{OM}_{variable,y}$ are the fixed and variable Operation and Maintenance (O&M) costs of the wind turbine per year and per MW. $mean(AEP)$ is the mean Annual Energy Production (AEP) of the wind power plant. $B^{E,OM}_y$ is the yearly O&M cost of the battery per MWh. In this study, we set a fixed lifetime for the battery (i_b) as battery degradation is not considered. Additionally, to address the decreasing costs of batteries over time, we employ the concept of equivalent number of present batteries (Nb_{eq}). This method incorporates the annual battery price reduction rate (f_b) and the designated replacement year for each battery ($y_b(i_b)$).

$$Nb_{eq} = \sum_{i_b=0}^{N_b-1} (1-f_b)^{y_b(i_b)}$$

described in Appendix C. It should be noted that the calculation of NPV/CAPEX requires only the HPP power output time series from either the ~~high fidelity~~ high-fidelity model or the surrogate.

4 Case Study

In Section 4.1, we ~~will~~ introduce the training and validation dataset. Following this, Section 4.2 ~~will discuss~~ discusses the data related to the intra-generalizability analysis. ~~Lastly, Section ?? will provide a detailed overview of~~ In Appendix C, the cost model ~~data specific to our application~~is presented, and the related data is provided in Table D2 of Appendix D.

4.1 Training and Validation Dataset

4.1.1 HPP configurations

As we rely on a surrogate to replace the high-fidelity EMS, we require a comprehensive dataset to train and validate this surrogate. Therefore, a wide range of HPP configurations ~~should~~ needs to be covered. In addition, these configurations ~~need to~~ must be realistic and in line with industry practices. Table 8 ~~summarize~~ summarizes the parameter ranges. For this article, the grid connection varies between 50 MW and 700 MW.

~~For this article, the grid connection varies between 50 MW and 700 MW.~~

To ensure an equal distribution of all variables across the entire parameter space, the Latin Hypercube Sampling ~~(LHS)~~ method, by Jin et al. (2005), ~~was~~ is used to randomly select 250 sizing configurations~~. Of~~ , of which 200 HPP (80%) are used to train the regressor and 50 HPP (20%) are used to evaluate the accuracy of the surrogate, as detailed in Section 2.2.2. Subsequently, the high-fidelity EMS ~~was~~ is solved using these configurations with the input time series presented in the section below.

4.1.2 Input time series & WT technology

The input time series required for the high-fidelity model, mentioned in Table 2, are generated using two tools. Wind power time series are simulated with the CorRES simulation tool (Murcia Leon et al., 2021; Koivisto et al., 2019). This tool is based on meteorological reanalysis data from the Weather Research and Forecasting model. CorRES' stochastic model (Koivisto et al., 2020b) ~~was~~ is integrated to add fluctuations, resulting in wind power time series with ~~15-minute-level~~ 15-minute resolution. The simulation ~~was~~ is based on meteorological data from the year 2012, with the assumption that the climate in 2030 remains unchanged from 2012. CorRES requires specific inputs~~are required~~, including the HPP's longitude, latitude, hub height of the wind turbine, power curve, and the simulation period. The considered turbine is the Gamesa G80 with a rated power of 2MW and a hub height of 100 meters.

SM price time series for the 2030 electricity markets are obtained from the Balancing Tool Chain (BTC) (Kanellas et al., 2020). BTC is built upon Balmorel, an open-source energy system model (Wiese et al., 2018) that simulates electricity market operations, ranging from day-ahead to real-time dynamics for the northern central European region. Additionally, an investment optimization is implemented to simulate a 2030 energy system scenario (Koivisto et al., 2020a). ~~The wind generation and price time series are presented in the figure below:~~

~~Input time series for each HPP configuration~~

4.1.3 Output time series

For all 250 HPP configurations ~~, and the above mentioned~~ and the aforementioned input time series, the high-fidelity model is used to generate all output time series described in ~~the~~ Table 4. Out of these HPP configurations, 200 are used for training the surrogate model~~and the~~ , and the remaining 50 ~~others~~ are used to validate the model.

4.2 Intra-generalizability analysis Data

For the intra-generalizability analysis, we use the best surrogate model following the methodology described in ~~Sections~~ Section 2.2. We then test the surrogate's accuracy across four randomly chosen locations within the same market region, labeled A to D. At each location, we randomly select 10 HPP configurations from the training dataset and another 10 from the validation dataset. The coordinates of each location are listed in Table D1. Figure 4 ~~a~~ displays these locations, indicating the training location with an "X" and the evaluation sites for the HPPs.

As all locations are in the same market region, the SM price time series is the same for all locations. The weather data for locations A-D ~~were~~ is provided by CorRES, and the output time series per location and per HPP configuration ~~were~~ are generated using the high-fidelity EMS model. This data is used to compare the performance of the surrogate trained on location X and evaluated on locations A-D.

The wind generation distribution across all locations ~~are available in Figure 4b. From this figure, it is observed that location C presents a different distribution than the other locations, notably with a lower average wind power . Meanwhile, locations~~ is available in Fig. 4. This violin plot illustrates the distribution of normalized wind power generation across five different

locations (X, A, B, ~~and D share similar distributions.~~ C, and D). Each half-violin represents the density of wind power measurements for a location, showing where values are most concentrated. The symmetrical nature of each violin plot, with mirrored halves for each location, is a standard feature of violin plots that allows for a clearer visualization of the data distribution, where each half represents the same distribution of wind power measurements. The width of each violin indicates the density: wider sections reflect more frequent occurrences of those power levels, while narrower sections suggest less common values. The plot uses a logarithmic scale on the y-axis, making it possible to visualize variations in power generation across a broad range, from very low to high outputs. Inside each violin, the black bar marks the interquartile range, while the white dot represents the median of the wind power measurements for that location. This combination allows for a clear comparison of both the range and central tendencies of wind power output across different sites. For example, a location with a narrower and higher median distribution might experience more consistent and higher wind power generation (i.e., location X), while one with a broader distribution and lower median could have more variability (i.e., location C). Locations A, B, and D share similar distributions where the shape of these distributions suggests that low power output is more common, with occasional rises to higher values.

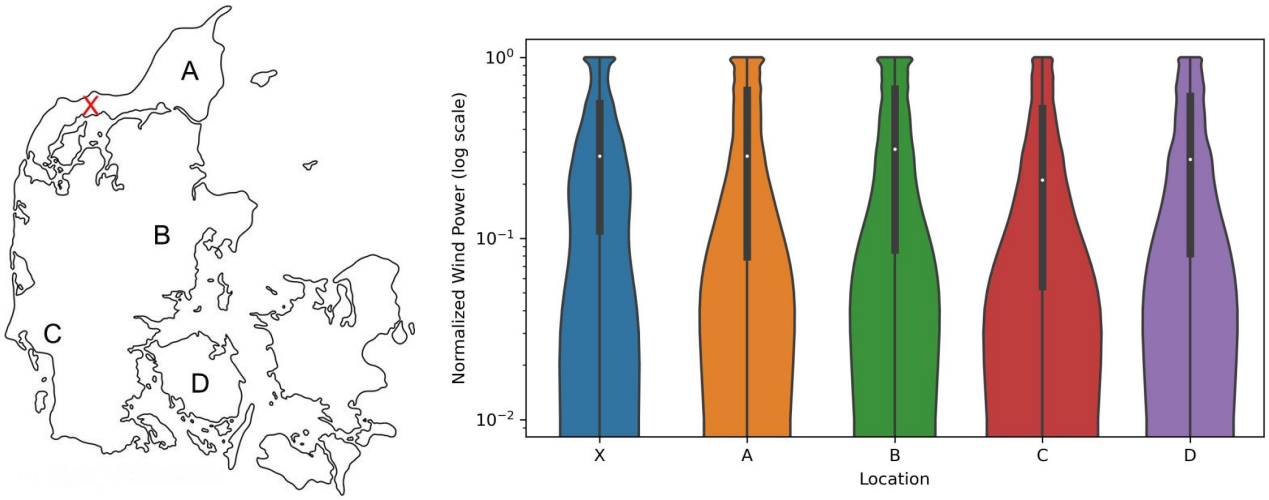

~~Intra-generalizability data~~

Figure 4. Intra-generalizability data. Left: location of trained surrogate model, X (in red) and evaluated model (A-D). Right: normalized wind power distribution across all locations. A log scale was used to highlight the difference between locations.

4.3 ~~Cost model Data~~

~~Table D2 presents a summary of the cost assumptions used in this article.~~

~~Cost assumptions Variable Value~~ r_{AT} ~~6%~~ τ_{tax} ~~22%~~ WT_{cost} ~~EUR/MW457, 143~~ WT_{civil} ~~EUR/MW185, 714~~ $WT^{OM}_{fixed,y}$ ~~EUR/MW/year9, 000~~ $WT^{OM}_{variable,y}$ ~~EUR/MWh/year0.964~~ B^{E}_{cost} ~~EUR/MWh90, 000~~ B^{P}_{cost} ~~EUR/MW32, 000~~ B^{P}_{civil} ~~EUR/MW36,~~

~~000 $B^{P}_{control}$ EUR/MW9, 000 $B^{E,OM}_{y}$ EUR/MWh/year0 f_b 10% i_b, lifetime of battery years7 Y, lifetime of HPP 25 HPP_{BOS} EUR/MW119,940 P^{G}_{cost} EUR/MW50,000~~

~~As the battery's lifetime is of 7 years, each HPP will require 3 batteries during its lifetime. Given a battery price reduction of 10% per year, we obtain a number of battery equivalent (Nb_{eq})of 1.84.~~

5 Surrogate Results

This ~~Section~~ section details the accuracy of the ~~surrogate models and their~~ best surrogate model and its main application in evaluating the ~~Profitability Index (PI) of Hybrid Power Plants (HPPs). We start by comparing the accuracy of each~~ PI of HPPs. The comparison of all surrogate models is provided in Appendix A. After introducing the results of the most accurate surrogate model in Section ~~??, followed by examining~~ 5.1, we examine how the accuracy of ~~the best surrogate model changes~~ that model varies with different training dataset sizes in Section 5.2. Next, in Section 5.3, we assess the surrogate's performance across various locations where it hasn't been trained. Finally, Section 5.4 compares the PI accuracy when evaluated using both the surrogate and the high-fidelity EMS. For all the results shown in this section, the validation dataset was used to evaluate the accuracy of the surrogate model and ~~the~~ its application.

5.1 Best Performing Surrogate ~~'s Accuracy for Hourly Operation~~Model

The ~~accuracy of the four models, presented~~ best-performing surrogate is the one titled S4 in Table 5~~, can be found in Figure A1. The RMSE of all hourly output time series is used to compare the accuracy of all models. This RMSE provides a holistic measure of the model's accuracy. Moreover, the training and inference time were reported in Table A1.~~

~~From Figure A1, it is observed that the tuned NN outperforms the linear counterpart~~ . From Fig. A1, we observe that all tuned NNs (S3 and S4) outperform their linear counterparts (S1 and S2) in terms of accuracy. This result is expected ~~as~~ to a certain degree: while the linear model ~~cannot capture the inherent non-linearities~~ may not fully capture the non-linear dynamics of the high-fidelity model, we selected it to assess the extent to which a simpler model can approximate the EMS, given that many of the HF EMS model's constraints are linear. Among the linear models, ~~using the~~ model S2, which uses SVD in addition to ~~the normalizationslightly outperforms the linear model using only the normalization. However, for tuned NNs, the opposite is true. Given the~~ normalization, slightly outperforms model S1, which uses only normalization. The application of SVD effectively captures key trends within the broad distribution of HPP configurations, ~~the SVD effectively captures key trends,~~ thereby improving the accuracy of the linear model ~~. Yet, when tuning comes into play, the NN~~ S2. However, we don't observe similar results when looking at the tuned models, S3 and S4. The NN of model S3 can make better use of all the data ~~(~~in the absence of SVD ~~) rather than~~ rather than using a reduced representation of it~~(when using the SVD)~~ , as in model S4, which explains the difference between both tuned FNNs.

~~Validation RMSE by Data Processing Method: "Linear" for multivariate linear regression, "NN_tune" for tuned FNN (parameters in Table 7), "Norm" for Normalization only, and "SVD" for combined Normalization and SVD methods.~~

~~Table A1 contrasts the time required to execute the workflow for each surrogate model. The pre-processing time considers both training and validation datasets. However, the training time accounts only for the training dataset, while the inference time reflect the inference on a single HPP configuration spanning one year of data.~~

~~Time Metrics of Surrogate Models **Method** **Model** **Pre-proc.** **Train Time** **Inf. Time** SVD Linear 7m 14m 0.02s SVD NN_Tuned 7m 5h 0.04s Normalization Linear 1.1m 14.4h 0.64s Normalization NN_Tuned 1.1m 7d 1.02s~~

There is a substantial difference between surrogates using ~~the normalization only and the surrogates using the~~ only normalization (S1 and S3) and those using SVD in addition to ~~the normalization~~ normalization (S2 and S4). This difference is even more ~~exacerbated when looking at NN_Tuned: when using SVDthe NN~~ pronounced when comparing the tuned neural network models: model S4 (with SVD) converges in 5 hours~~while it~~, whereas model S3 (without SVD) takes 7 days ~~for the surrogate employing only a normalization. This~~ to converge. This disparity is mainly due to the difference in training data dimensionality, as highlighted in Table 6. The use of SVD reduces the number of features, simplifying the model and accelerating the training process with very little compromise on accuracy.

~~From both presented figure and~~ Based on the results presented in both the figure and the table, we conclude that the tuned ~~FNN using the SVD~~neural network using SVD—model S4—provides the best ~~compromises~~ compromise between accuracy, training time, and execution time.

To gain deeper insights into ~~this surrogate's performance~~ the performance of model S4, we investigated its capability to ~~predict each~~ approximate each normalized hourly output time series individually ~~, for~~ across all validation data. Figure 5 provides ~~such an overview~~ an overview of these results. From this figure~~we observed~~, we observe that the power output of the HPP and the curtailed power are well ~~predicted, however~~ estimated by the surrogate model. However, the battery charge and discharge profiles are ~~harder to predict~~more challenging to compute accurately. To further understand these discrepancies, we examine the ~~predicted~~ calculated output time series for a given day ~~,~~ from the surrogate, as well as the ~~observed~~ corresponding output time series from the ~~high fidelity~~ high-fidelity model.

Figure 6 shows the difference between the ~~the~~ surrogate's ~~prediction and the ideal behavior, from the high-fidelity model.~~

~~Output time series for a given day, from the high-fidelity model (blue) and the surrogate (red). All time series are in MegaWatt.~~

approximation and the HF EMS' outputs. The surrogate captures ~~well~~ the daily trend well across all time series. While it accurately ~~predicts~~ estimates the intra-day fluctuations for power bidding, it is less precise when ~~predicting~~ estimating battery charge and discharge power. This is due to the abrupt power fluctuations ~~,~~ in the high-fidelity model, ~~that can be seen in Figure 6b and 6c~~as seen in Fig. 6(b) and 6(c). Additionally, as shown in ~~Figure~~ Fig. 6d, the surrogate occasionally struggles to ~~forecast~~ approximate consistent zero values over an entire day—a challenge characteristic of FNNs. Nonetheless, these discrepancies are minor, with ~~predicted~~ estimated curtailed power fluctuating within a ± 1.5 MW range instead of the expected steady 0 MW. Such variances are negligible relative to the HPP's export capacity, which can reach up to 700 MW.

The application presented in Section 3, requires only the HPP power output out of all the ~~predicted~~ calculated output time series. That is why we ~~want to~~ further examine this output time series. ~~Figure 7 a~~ The left panel of Fig.7 presents a hexbin plot that compares hourly ~~predicted~~estimated, and normalized, HPP power outputs across all HPP configurations in the validation

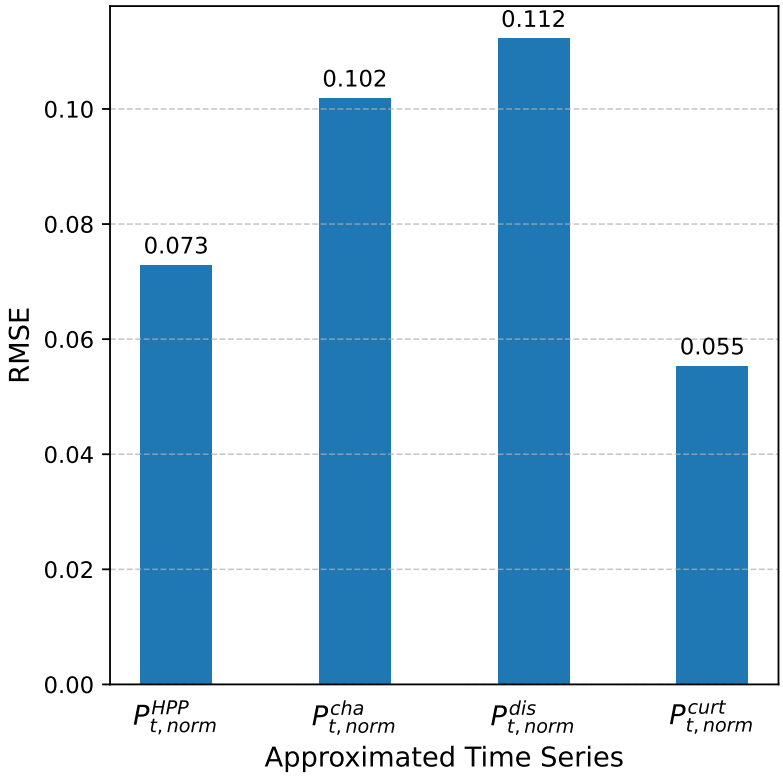

Figure 5. RMSE for each surrogate's output time series across all validation HPP configurations. ~~P_HPP_SM is~~ For the ~~power bidding on the SM. P_cha_RT and P_dis_RT are the charging and discharging power~~ definition of ~~the battery~~each variable, refer to Eq. ~~RES_RT_cur is the curtailed power.~~1 to 4

dataset ($P^{HPP}_{Surrogate}$). The hexagonal bins group nearby points (denoted as count in Fig. 7(a)) and show the density of data points within each bin. The ~~value of the density~~ density value is shown on the color bar~~,~~; the darker the color, the denser the hexagon. A log scale is used for clarity. A one-to-one line, representing ~~an ideal prediction~~a perfect model, is also depicted for comparison. The power bidding on the SM aligns closely with the observed values (P^{HPP}_{EMS}).

The PDF of errors ~~,~~ for the same data ~~, is shown in Figure 7b~~is shown on the right-hand side of Fig. 7. The histogram (in blue) shows the frequency distribution of these errors, while the red line represents a Gaussian (normal) distribution fitted to the data. The parameters of the Gaussian fit—mean (μ) and standard deviation (σ)—are shown in the legend and are ~~both approximately~~ 0.00 and 0.07, respectively. The RMSE is also 0.07, indicating the typical magnitude of ~~prediction~~ computation errors.

The mean (μ) being ~~close~~ equal to zero suggests that the surrogate's ~~predictions~~ calculations are unbiased on average. The Gaussian fit's close alignment with the histogram suggests that the errors are distributed in a manner consistent with a normal distribution, which often implies that the surrogate model's residuals are well-behaved in a statistical sense.

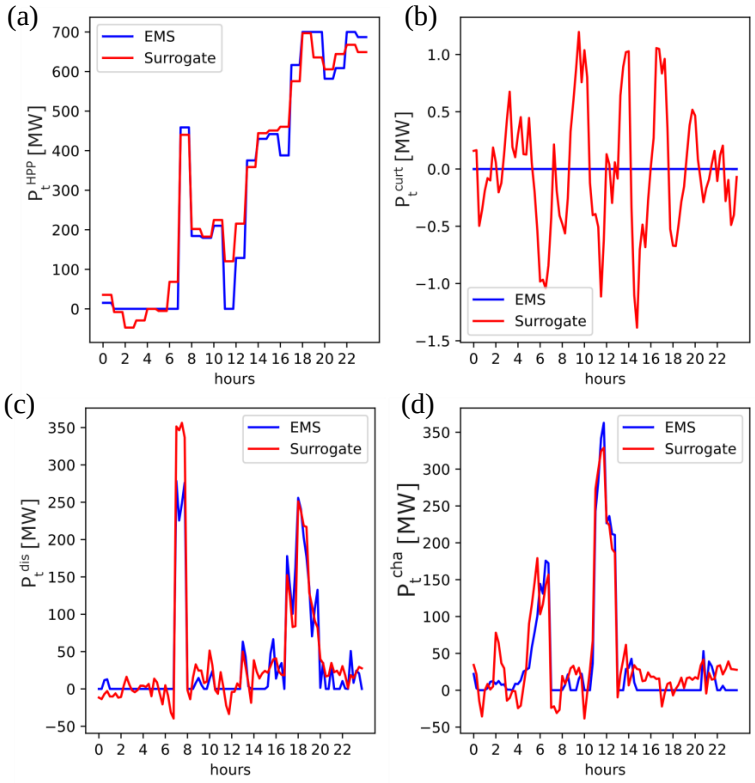

Figure 6. Output time series for a given day, from the high-fidelity model (blue) and the surrogate (red). All time series are in MW. (a): power output of the HPP, (b): battery charge profile, (c): battery discharge profile, (d): curtailed power

5.2 Surrogate Convergence to Training Dataset

The previous study ~~has~~ demonstrated the capacity of the NN to replicate the daily trends of the high-fidelity ~~NN~~EMS. However, the chosen data was based on an arbitrarily ~~high~~ large number of HPP configurations. Consequently, we sought to examine how the NN's accuracy varies with different dataset sizes. ~~NNs were tuned using the SVD processing, with a training dataset~~ Several surrogates were trained based on model S4 with varying training dataset sizes, ranging from 4 to 200 HPP configurations. The validation dataset from the previous study is not modified to ~~provide~~ ensure a fair comparison. Results of these simulations are illustrated in ~~Figure~~ Fig. 8. Interestingly, the RMSE seems to plateau when reaching a training dataset size of 110 HPP configurations. We also note that there is only a marginal gain in accuracy between 50 and 100+ HPP configurations. This is relevant ~~to highlight as~~ because it suggests potential reductions in the ~~generated data~~ data generated by the high-fidelity EMS, and, therefore~~shorter training duration~~ , shorter training durations for the surrogate. As a reminder, each HPP configuration, which spans ~~over~~ one year of data, requires 47 minutes to generate outputs using the high-fidelity EMS. It is also interesting to compare the Normalized Root Mean Square Error (NRMSE) of yearly revenues, computed as per ~~equation~~ Eq. 6. The

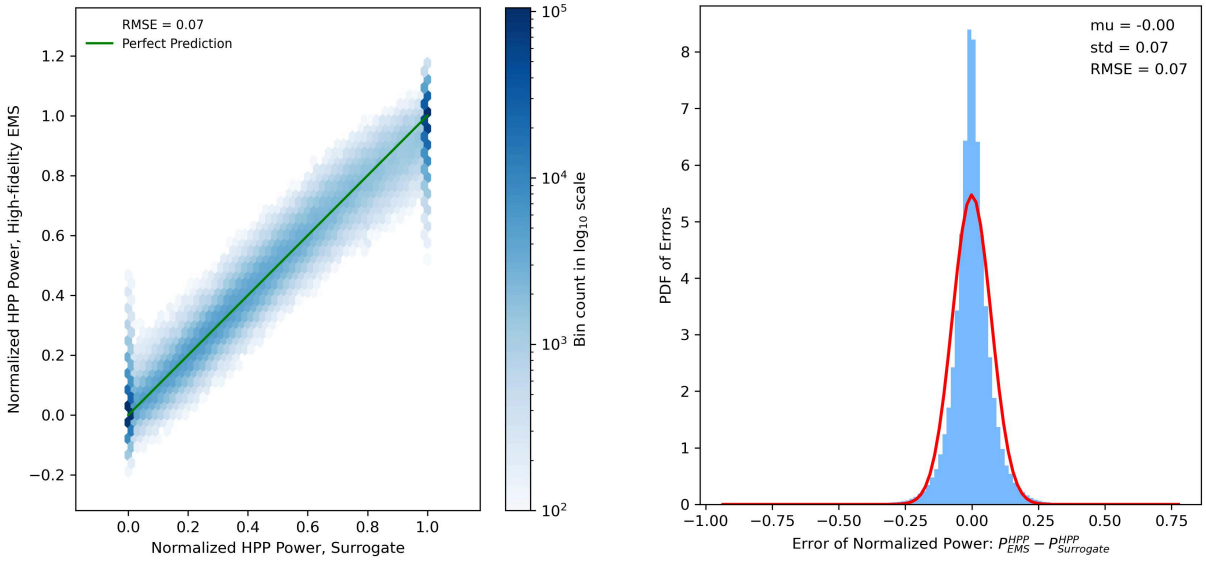

Figure 7. Accuracy ~~and error distribution~~ of model S4 in approximating hourly normalized ~~Power Output~~power output (see Eq. 1) for all HPP from the validation dataset. Left: the hexbin plot, group nearby points and show the density of data points within each bin, refer to the colorbar for the density of each bin. Right: PDF of error, the red line indicates a Gaussian fit, with parameters detailed in the legend.

model trained with 200 HPP configurations has an NRMSE of 0.81%~~while the the~~ , while the model trained with 32 HPP configurations has an NRMSE of 1.0% across the entire validation dataset. ~~Here again~~Again, the difference between both outcomes is marginal, suggesting further reductions in training time and during the data generation process.

5.3 Intra-generalizability Accuracy

~~In the section~~n this section, we evaluate the surrogate ~~'s accuracy on~~ accuracy of model S4 at four different locations (A to D). ~~The selected surrogate is the tuned FNN using the SVD whose results were~~ Surrogate S4 is the one whose results are detailed in Section ~~??~~5.1. As a reminder, this surrogate is trained using weather data from location X and with a training dataset of 200 HPP configurations. As a reminder, this surrogate is trained using weather data from location X and with a training dataset of 200 HPP configurations. We use the NRMSE of yearly revenues to measure the accuracy of the surrogate at each location. This was done on 10 randomly selected HPP configurations from the training dataset and 10 others from the validation dataset. All accuracy results are compared to the baseline~~e.g.~~, i.e., using location X. The accuracy of the surrogate is illustrated in ~~Figure~~ Fig. 9.

The surrogate model's NRMSE for ~~predicting revenue demonstrates~~ computing revenue shows a marginal difference between training and validation datasets. Specifically, the NRMSE for the training dataset (location X) is 0.79%, compared to 0.81% for the validation dataset. When looking at ~~location~~ locations A to D, the average NRMSE for the training dataset

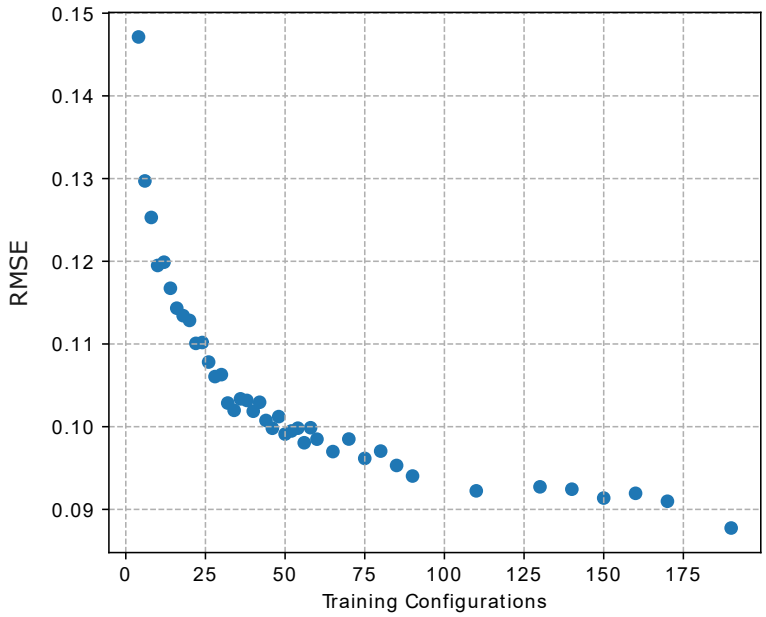

Figure 8. Evolution of accuracy with increasing training dataset size. A fixed validation dataset, of 50 configurations, is used across all simulations.

samples is 0.79% (aligning with the Train Baseline), whereas it is 1.3% for validation dataset samples. Notably, location D shows the greatest discrepancy in NRMSE between training and validation samples. This variation may be attributed to the combination of HPP configurations and distinct weather time series at location D, ~~detailed in Figure 4b. Overall~~as detailed in Fig. 4. Overall, despite location X's distribution with two distinct peaks (around 0.08 and 0.1) that aren't observed in other locations, the surrogate's performance remains consistent across all locations.

5.4 PI Evaluation Accuracy

In this section, we evaluate the PI of several HPPs using the surrogate S4 (presented in Section 5.1) and the high-fidelity EMS model. Both frameworks are described in ~~Figure 3. In order to~~ Fig. 3. To evaluate the accuracy of the PI computed with the surrogate, we use the same 50 HPP configurations ~~,~~ from the validation dataset ~~,~~ for both frameworks. ~~The selected surrogate is the tuned FNN using the SVD described in Section ??.~~ Figure 10 shows the PI calculated using the high-fidelity EMS on the y-axis and the PI inferred using the surrogate on the x-axis for the corresponding HPP configuration.

The RMSE of PI across the validation dataset is ~~of~~ 0.010, ~~which indicates~~ indicating the average magnitude of the errors between the surrogate~~predictions~~ 's estimations and the high-fidelity EMS evaluations. The scatter plot shows that most ~~of the~~ points are close to the line of perfect ~~prediction~~ calculations (red line), with some scatter around it. Most ~~of the~~ points are below the perfect line, indicating that the surrogate ~~is slightly overestimating~~ slightly overestimates the profitability of the HPP. However, this tendency is reversed for higher NPV/CAPEX, where the surrogate provides a conservative estimate of the

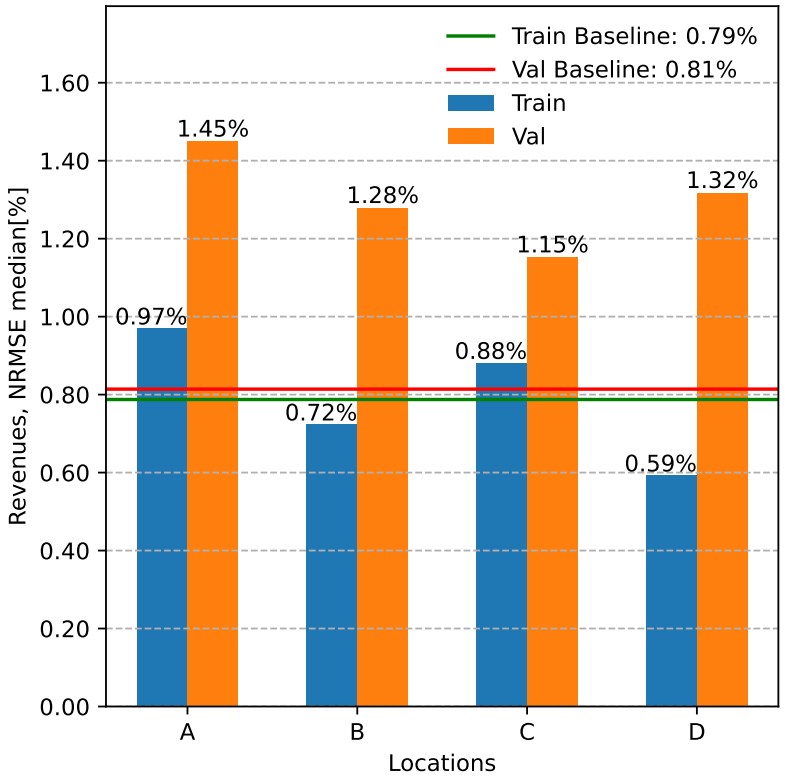

Figure 9. Performance of surrogate S4's generalizability for different locations and for HPP configurations from different datasets. The Baseline refers to location X, where the surrogate has been trained. Train Baseline and Val Baseline correspond to the NRMSE of Revenues from the training dataset of location X (200 HPP configurations) and from the validation dataset (50 HPP configurations). Val refers to 10 HPP configurations randomly selected from the validation dataset, while Train refers to 10 random HPP configurations from the training dataset. Both Val and Train are evaluated on ~~location~~ locations A-D.

PI. Overall, the tight clustering of points around the red line suggests that the surrogate model is ~~quite reliable for predicting~~ reliable for computing the PI when compared to the high-fidelity EMS.

6 Discussion

This study aims to evaluate the potential of applying surrogate modeling ~~in order~~ to emulate the behavior of a complex EMS for ~~a~~ an HPP with bidding on the spot market. Given the increasing integration of renewable energy systems — particularly wind power — this research provides a practical approach to optimize HPP operations, enabling more efficient system integration and financial assessment.

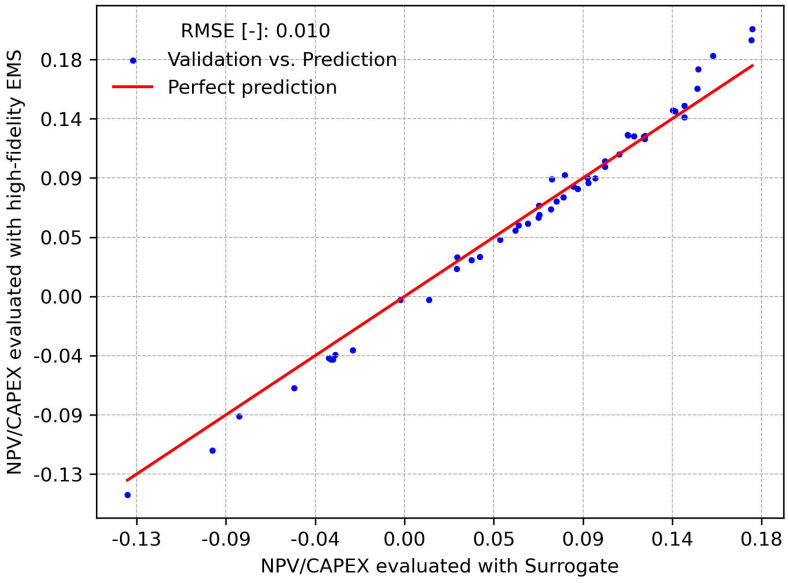

Figure 10. PI comparison based on surrogate inference and high-fidelity EMS evaluation for the validation dataset.

Our investigation highlights the importance of both pre- and post-processing of data with an appropriate choice of the surrogate model. Among the options explored, the tuned FNN that utilizes SVD (surrogate S4) emerged as the optimal balance. Indeed, ~~Figure~~ Fig. A1 shows that the tuned NN using only ~~a normalization~~ normalization (surrogate S3) is the most accurate, while adding ~~an SVD results in a~~ SVD (surrogate S4) results in similar performance. Yet, when we look at the computational time, as shown in Table A1, using ~~the SVD~~ SVD (in surrogates S2 and S4) significantly reduces the training duration. This difference is even more pronounced when the tuning time is considered: it requires five days to tune the NN using ~~a normalization~~ normalization (surrogate S3), whereas it takes ~~only~~ 4.3 hours when ~~an SVD~~ SVD (surrogate S4) is used. This discrepancy is ~~assigned~~ attributed to the inherent capability of ~~the~~ SVD to extract a reduced order of data that contains meaningful coefficients and daily temporal trends.

However, challenges persist, particularly in ~~predicting~~ estimating battery charge and discharge profiles. As depicted in ~~Figures~~ Fig. 5 and 6, this difficulty arises from the ~~high fidelity~~ high-fidelity model's abrupt power output fluctuations and the intrinsic non-linearity of these variables. ~~For the~~ In particular, Fig. 6(c) and (d) highlight the surrogate's limitations in accurately and consistently representing the battery's hourly operation. In several time steps, the model shows the battery charging and discharging simultaneously, and at times, the charge and discharge power take on negative values, which is physically unrealistic. These issues stem from the nature of the regressor; the FNN cannot inherently capture the physical constraints that would typically be enforced by multiple equations. Specifically, the FNN lacks explicit equations to govern its outputs. However, for the purposes of this study, focusing primarily on the power output of the HPP is sufficient, as this is the only variable required in revenue calculation and subsequent ~~profitability index~~ PI evaluation. Additionally, the power output of the HPP is well ~~predicted~~ estimated, as shown in ~~Figure 7b~~the PDF plot of Fig. 7: there is no bias, and the standard deviation

is very small. While this result only ~~stands~~ holds for a surrogate trained with 200 HPP configurations, it is still reasonable to assume similar behavior for a surrogate trained with ~~less~~ fewer data points. Indeed, ~~Figure 8 demonstrate~~ Fig. 8 demonstrates a marginal difference in accuracy between a surrogate trained with 200 HPP configurations and one trained with 50 HPP configurations. Ultimately, it is a ~~trade off~~ trade-off between training time and accuracy. In terms of intra-regional generalizability, the accuracy across different locations is more consistent than between dataset types. This uniformity in accuracy ~~,~~within each dataset type ~~,~~can be partly attributed to the region's relatively homogeneous wind profiles, facilitated by its largely flat terrain. A loss in accuracy is observed when unseen HPP configurations are used (e.g., validation dataset). Nonetheless, these results demonstrate the surrogate's ability ~~in capturing~~ to capture essential data trends (~~Figure~~ Fig. 9). However, it is important to note that this study's scope was confined to the DK1 market region, characterized by uniform wind profiles due to its flat terrain (~~Figure 4b~~Fig. 4). The fast and accurate surrogate allows us to evaluate ~~a~~ an HPP's profitability throughout its lifetime with little computational burden. Indeed, the surrogate model is capable of evaluating the NPV/CAPEX for all 50 HPP configurations ~~of Figure 10 in a mere~~ in Fig. 10 in 25 seconds. In contrast, computing the same evaluations using the high-fidelity model for each HPP configuration, with inputs spanning over a year, would take approximately 39 hours. However, it is important to understand the impact of the surrogate's accuracy on the ~~the~~ PI. Figure 10 shows that the surrogate can be reliably used if slight ~~deviation of the order of magnitude of~~ deviations of around 0.010 in the PI are acceptable for the intended business evaluation. In other words, the error on the ~~predicted~~ computed NPV is around 1% of the CAPEX. It is also relevant to note that not all HPP configurations are profitable, resulting in negative PI~~and~~ , further supporting the use of NPV/CAPEX as an evaluation metric. Hence, the importance of optimization in the context of ~~sizing of HPP~~ HPP sizing, which is enabled with the developed framework. However, a detailed exploration of the sizing optimizer is beyond the scope of this manuscript and will be the subject of future investigations. It is important to emphasize that these findings are site-specific and heavily dependent on the cost model employed~~, hence~~; hence, they should not be generalized across different HPP sites.

There are certain limitations and future works worth acknowledging. For one, ~~The~~ the full capabilities of the high-fidelity model ~~has~~ have not been leveraged. While the EMS can consider a ~~realisation~~ realization of the forecast error in both weather and market data, our initial approach prioritized a methodology using perfect forecast data. Nonetheless, this is a natural next step, where a sizing framework can be developed based on a surrogate that can handle the inherent uncertainties in weather and market forecast errors. While our research ~~was~~ mainly focused on the spot market, currently the major source of revenues for power plants, ~~the~~ market dynamics might shift. As the share of intermittent power ~~plant~~ plants increases in the grid system~~that~~ , which is becoming more decentralized, the balancing market is forecasted to become a considerable revenue stream. Thus, there is a pressing need for a more comprehensive surrogate considering operational strategies in both spot and balancing markets. ~~Moreover, a FNN has it's own limitation~~ Moreover, an FNN has its own limitations when it comes to time series representation, as seen in the battery charge and discharge profiles ~~on Figure~~ in Fig. 6. This highlights the importance of further exploring the machine learning field. A promising avenue would be models that blend physical constraints, such as physics-informed neural networks. Additionally, to develop a more robust sizing methodology, it is necessary to account for various forecast scenarios for wind generation and market prices within the EMS. This can be achieved through methods from the field of surrogate-based optimization under uncertainty. These considerations will be addressed in future work.

7 Conclusion

In this paper, we have introduced a new methodology to accurately and efficiently approximate a ~~state of the art EMS for HPP~~ state-of-the-art EMS for HPPs involved in spot market power bidding. This model leverages singular value decomposition to extract temporal trends in the input ~~, and utilizes FNN,~~ and utilizes an FNN to represent the non-linear dynamics of the EMS. This method has demonstrated over twice the accuracy of traditional multivariate linear regression models. A key innovation of our study is the ~~synergistic~~ combined use of SVD and FNN, ~~a combination that represents a first~~ which represents a novel approach in this field. This approach successfully replicates the annual revenues of an HPP with an NRMSE of 0.81% for the best model. To fully demonstrate the capabilities of our surrogate model, we have integrated it into a sizing evaluation framework designed to calculate the Profitability Index (~~NPV/CAPEX~~$NPV/CAPEX$) based on the technology mix rating within the HPP. This framework not only enabled substantial computational savings—reducing processing time from 39 hours to ~~a mere~~ 25 seconds compared to a high-fidelity model—but also ~~maintained remarkable accuracy with~~ achieved an RMSE of 0.010. ~~Though our methodology may seem~~ Although our methodology is straightforward, it is nonetheless powerful and opens up new possibilities ~~in the field of HPP sizing optimization~~for optimizing HPP sizing in the context of renewable energy integration. This study emphasizes the relevance of surrogate modeling to the wind energy field, where efficient and accurate tools are essential for navigating the increasing complexity of renewable energy markets and supporting the transition toward sustainable energy systems.

Data availability. The weather and spot market price time series data are available on request from the corresponding author.

Table 1. Comparison of HF and LF EMS Models

Aspect	HF EMS	LF EMS
Component modeling	Physical modeling per component considering the electrical, mechanical, and/or thermal behaviors. Includes battery degradation model	Simplified or aggregated model, linear approximations or average values used for component performance
Market Participation Modeling	Complex bidding strategies in various electricity markets (day-ahead~~market, including regulatory periods of the Danish market structure. To account for the uncertain nature of wind speed and market prices, Crespo-Vazquez et al. (2018) formulated a two-stage convex stochastic programming framework that incorporates stochastic variables for day-ahead prices, balancing market prices, and power bidding . Several other studies have contributed to the field, formulating optimization problems under stochastic conditions (Abhinav and Pindoriya, 2021; Fang and Zhao, 2020; Huang et al., 2021a) and deterministic scenarios (Cai et al., 2016b). However, these formulations typically assume a given HPP configuration with fixed sizes for wind turbines and battery capacity,optimizing the system's operation within these constraints. Optimal sizing of an HPP, on the other hand, requires variations in the sizes of the wind turbines and battery energy and power, presenting a more complex challenge . Consequently, sizing an HPP based on any comprehensive and realistic EMS models involves running the EMS optimization~~, intraday, balancing), includes market rules and regulations (i.e., dispatch and settlement intervals), and/or grid compliance requirements	Usually focuses on one market, ignoring opportunities or penalties from other markets
Input data and Forecast	Varying resolution (from sub-hourly to hourly). Possible combination of forecast and real-time data	Uses hourly resolution. Deterministic forecasts or perfect forecast

Table 2. Inputs and Outputs of ~~EMS~~ SM optimization and ~~PMS~~ RT dispatch from Zhu et al. (2022).~~RT stands for Real-Time.~~

Model	Inputs	Outputs
SM optimization	HPP configuration	HPP power output schedule
	Wind power forecast	Battery charge/discharge power
	SM price forecast	Battery state of charge
RT dispatch	Same as ~~EMS~~SM optimization, and	RT HPP power output
	RT wind power	RT battery charge/discharge power
	Cleared SM prices	RT battery state of charge
	~~EMS~~ SM optimization power output schedule	RT curtailed power

Table 3. ~~Annual~~ Computational Complexity of HF EMS~~and PMS~~' models for one year of input data

Model	Design variables	Constraints
~~EMS~~ SM optimization	289,445	350,765
~~PMS~~ RT dispatch	315,360	420,480

Table 4. Input and output time series of surrogate models

	Variable	Time step	Time horizon
Input	SM price forecast: SM_t Wind power forecast: W_t	15 min	1 day
Output	HPP power output: ~~P_t^{sm}~~ P_t^{HPP} Battery discharging power: ~~$P_t^{sm,dis}$~~ P_t^{dis} Battery charging power: ~~$P_t^{sm,cha}$~~ P_t^{cha} HPP curtailed power: ~~$P_t^{sm,curt}$~~ P_t^{curt}	1 hour	1 day

Table 5. Surrogate models tested

Model Name	Pre-processing	Regressor	Post-processing
S1	Normalization	Linear	Reverse Normalization
S2	Normalization SVD	Linear	Reverse SVD Reverse Normalization
S3	Normalization	FNN	Reverse Normalization
S4	Normalization SVD	FNN	Reverse SVD Reverse Normalization

Table 6. Features and Samples of Data-processing methods

Data processing		Normalization	SVD
Inputs	Features	5	$r_{in} + 3$
	Samples	$(24 \cdot 2) \cdot 365 \cdot N$	$365 \cdot N$
Outputs	Features	4	r_{out}
	Samples	$(96 \cdot 4) \cdot 365 \cdot N$	$365 \cdot N$

Table 7. FNN grid search hyperparameter space

Hyperparameter	Range	Step
Layers	[3,9]	1
Neurons per layer	[40,80]	20

Table 8. Sizing Parameters and Ranges

Sizing Parameter	Range
P^W/P^G [-]	[1, 2]
B^P/P^G [-]	[0, 1]
B^E/B^P [h]	[1, 8]

Appendix A: Surrogate Models Comparison

The accuracy of the four models, presented in Table 5, can be found in Fig. A1. The RMSE of all normalized hourly output time series is used to compare the accuracy of the models. Moreover, the training and inference times are reported in Table A1.

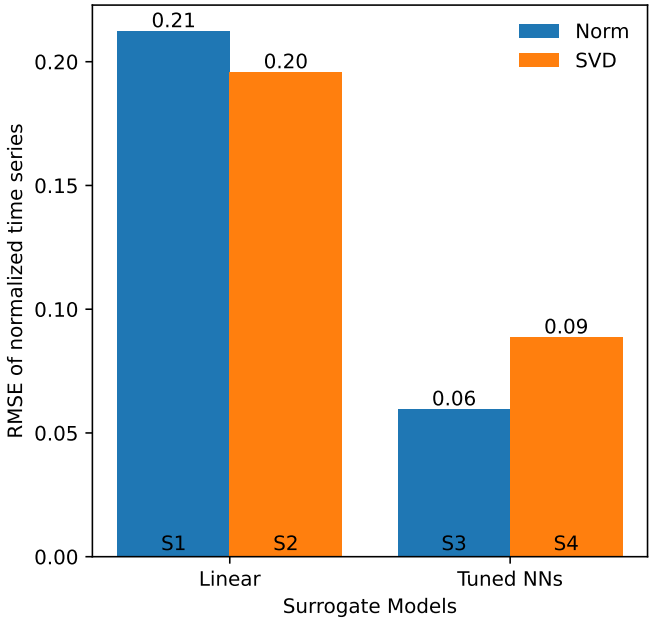

Figure A1. Validation RMSE by Data Surrogate model: "Norm" for models using a normalization only, and "SVD" for models using a combined normalization and SVD.

Table A1 compares the time needed to execute the methodology for each surrogate model. The pre-processing (Pre-proc.) time considers both training and validation datasets. However, the training time (Train Time) accounts only for the training dataset, while the inference time (Inf. Time) reflects the inference on a single HPP configuration spanning one year of data.

Table A1. Time Metrics of Surrogate Models

Model Name	Pre-proc.	Train Time	Inf. Time
S1	1.1m	14.4h	0.64s
S2	7m	14m	0.02s
S3	1.1m	7d	1.02s
S4	7m	5h	0.04s

Appendix B: FNN architecture

Tables with tuned FNN architecture.

Table B1. Architecture of ~~tuned NN using SVD~~model S4

Layers	Neurons
Input Layer	17
Hidden Layer 1	80
Hidden Layer 2	60
Hidden Layer 3	80
Hidden Layer 4	80
Hidden Layer 5	80
Hidden Layer 6	80
Hidden Layer 7	60
Hidden Layer 8	80
Hidden Layer 9	80
Output Layer	125

Table B2. ~~Place holder:~~ Architecture of ~~tuned NN using a normalization~~model S3

Layers	Neurons
Input Layer	5
Hidden Layer 1	80
Hidden Layer 2	80
Hidden Layer 3	80
Hidden Layer 4	80
Output Layer	4

Appendix C: Cost Model

The cost model is described in this section. The CAPEX depends on C_w, C_b, and C_{el}, which are the CAPEX of the wind power plant, batteries, and the Balance of System (BOS). Similarly, the OPEX is the sum of $O_{w,y}$, $O_{b,y}$, and $O_{el,y}$, which are the yearly OPEX from the wind power plant, batteries, and BOS. C_w is proportional to the wind turbine's cost (WT_{cost})

and the cost of civil works (WT_{civil}) in $EURo/MW$. Meanwhile, C_{el} is proportional to a combination of the number of battery equivalents in today's value (Nb_{eq}), the battery energy cost per MWh (B^E_{cost}), the battery power cost (B^P_{cost}), civil costs (B^P_{civil}), and control system costs ($B^P_{control}$) per MW. C_{el} depends on the shared BOS cost (C_{BOS}), the grid connection cost of the HPP (P^G_{cost}), and the cost of land in $Euro/km^2$ (L_{rent}) . The OPEX of the wind power plant is calculated based on the fixed and variable Operation and Maintenance (O&M) costs of the wind turbine per year and per MW ($WT^{OM}_{fixed,y}$ and $WT^{OM}_{variable,y}$), as well as the mean Annual Energy Production (AEP) of the wind power plant ($mean(AEP)$). Meanwhile, the battery's yearly OPEX is proportional to the yearly O&M cost of the battery per MWh ($B^{E,OM}_y$). The equations are as follows:

$$CAPEX = C_w + C_b + C_{el}$$

$$OPEX_y = O_{w,y} + O_{b,y} + O_{el,y}$$

$$C_w = (WT_{cost} + WT_{civil}) \cdot P^W$$

$$C_b = Nb_{eq} \cdot B^E_{cost} \cdot B^E + (B^P_{cost} + B^P_{civil} + B^P_{control}) \cdot B^P$$

$$C_{el} = (C_{BOS} + P^G_{cost}) \cdot P^G + L_{rent}$$

$$O_{w,y} = WT^{OM}_{fixed,y} \cdot P^W + mean(AEP) \cdot WT^{OM}_{variable,y}$$

$$O_{b,y} = B^{E,OM}_y \cdot B^E$$

$$O_{el,y} = 0$$

In this study, we set a fixed lifetime for the battery (i_b) as battery degradation is not considered. Additionally, to address the decreasing costs of batteries over time, we employ the concept of the equivalent number of present batteries (Nb_{eq}). This method incorporates the annual battery price reduction rate (f_b) and the designated replacement year for each battery ($y_b(i_b)$).

$$Nb_{eq} = \sum_{i_b=0}^{N_b-1} (1 - f_b)^{y_b(i_b)}$$

Appendix D: Data supplement

Table with the coordinates of each location used in the intra-generalizability study.

Table D2 presents a summary of the cost assumptions used in this article. As the battery's lifetime is seven years, each HPP will require three batteries during its lifetime. Given a battery price reduction of 10% per year, we obtain an equivalent number of batteries (Nb_{eq}) of 1.84.

Table D1. Location Coordinates for the Generalizability study. Coordinates are shown in decimal degrees.

Location	Latitude	Longitude
X	57.0482	8.8876
A	56.383	8.6705
B	55.2908	8.6551
C	57.1852	9.9527
D	55.3088	10.4398

Table D2. Cost assumptions

Variable	Value
r_{AT}	6%
τ_{tax}	22%
WT_{cost} [MEUR/MW]	0.46
WT_{civil} [MEUR/MW]	0.19
$WT^{OM}_{fixed,y}$ [MEUR/MW/year]	9,000
$WT^{OM}_{variable,y}$ [EUR/MWh/year]	0.97
B^{E}_{cost} [EUR/MWh]	90,000
B^{P}_{cost} [EUR/MW]	32,000
B^{P}_{civil} [EUR/MW]	36,000
$B^{P}_{control}$ [EUR/MW]	9,000
$B^{E,OM}_{y}$ [EUR/MWh/year]	0
f_b	10%
i_b, lifetime of battery [years]	7
Y, lifetime of HPP	25
C_{BOS} [MEUR/MW]	0.12
P^{G}_{cost} [MEUR/MW]	0.05

Author contributions. C.A., J.P.M.L. and K.D., conceived the research, C.A., J.P.M.L., and J.Q., developed the methodology C.A. and J.P.M.L. developed the code for the surrogate and gathered the required data, C.A., J.P.M.L., J.Q., and T.G., performed the formal analysis, J.P.M.L., K.D., S.G., and T.G. supervised the work, C.A., J.P.M.L., and J.Q., wrote the original draft and J.P.M.L., K.D., S.G., and T.G reviewed and suggested modifications for the draft.

Competing interests. The authors declare that they have no conflict of interest.

Disclaimer. This work is funded by TotalEnergies under the project "Hybrid Power Plant Life-cycle Optimization".

Acknowledgements. We would like to thank Juan-Andrés Pérez-Rúa and Poul Ejnar Sørensen for their critical feedback on the methodology and the figures as well Jenna Iori for her feedback after the first draft was written, and finally Rujie Zhu for sharing the high-fidelity EMS script.

References

Abdeltawab, H. H. and Mohamed, Y. A. R. I.: Market-oriented energy management of a hybrid wind-battery energy storage system via model predictive control with constraint optimizer, IEEE Transactions on Industrial Electronics, 62, 6658–6670, https://doi.org/10.1109/TIE.2015.2435694, 2015.

Abhinav, R. and Pindoriya, N. M.: Risk-constrained optimal bidding strategy for a wind power producer with battery energy storage system using extended mathematical programming, IET Renewable Power Generation, 15, 689–700, https://doi.org/10.1049/rpg2.12058, 2021.

An, Y., Zhao, Z., Wang, S., Huang, Q., and Xie, X.: Coordinative optimization of hydro-photovoltaic-wind-battery complementary power stations, CSEE Journal of Power and Energy Systems, 6, 410–418, https://doi.org/10.17775/CSEEJPES.2019.00330, 2020.

Barbosa, A. M., Rotella Junior, P., Rocha, L. C. S., Barbosa, A. d. S., and Bolis, I.: Optimization methods of distributed hybrid power systems with battery storage system: A systematic review, https://doi.org/10.1016/j.est.2024.112909, 2024.

Bhatt, P., Kumar, Y., and Soulaïmani, A.: Deep convolutional architectures for extrapolative forecasts in time-dependent flow problems, Advanced Modeling and Simulation in Engineering Sciences, 10, 1–35, https://doi.org/10.1186/S40323-023-00254-Y/TABLES/15, 2023.

Busch, S., Kasdorp, R., Koolen, D., Mercier, A., and Spooner, M.: The Development of Renewable Energy in the Electricity Market, Tech. Rep. KC-BD-23-004-EN-N, European Commission, https://doi.org/10.2765/411281, 2023.

Cai, Z., Bussar, C., Stöcker, P., Moraes, L., Magnor, D., and Sauer, D. U.: Optimal Dispatch Scheduling of a Wind-battery-System in German Power Market, Energy Procedia, 99, 137–146, https://doi.org/10.1016/J.EGYPRO.2016.10.105, 2016a.

Cai, Z., Bussar, C., Stöcker, P., Moraes, L., Magnor, D., and Sauer, D. U.: Optimal Dispatch Scheduling of a Wind-battery-System in German Power Market, Energy Procedia, 99, 137–146, https://doi.org/10.1016/j.egypro.2016.10.105, 10th International Renewable Energy Storage Conference, IRES 2016, 15-17 March 2016, Düsseldorf, Germany, 2016b.

Council of the European Union: Electricity Market Reform: Council Signs Off on Updated Rules, https://www.consilium.europa.eu/en/press/press-releases/2024/05/21/electricity-market-reform-council-signs-off-on-updated-rules/, accessed: 2024-10-09, 2024.

Crespo-Vazquez, J. L., Carrillo, C., Diaz-Dorado, E., Martinez-Lorenzo, J. A., and Noor-E-Alam, M.: A machine learning based stochastic optimization framework for a wind and storage power plant participating in energy pool market, Applied Energy, 232, 341–357, https://doi.org/10.1016/j.apenergy.2018.09.195, 2018.

Das, K., Hansen, A. D., Koivisto, M., and Sørensen, P. E.: Enhanced features of wind-based hybrid power plants, Proceedings of the 4th International Hybrid Power Systems Workshop, 2019.

Das, K., Philippe Grapperon, A. L. T., Sørensen, P. E., and Hansen, A. D.: Optimal battery operation for revenue maximization of wind-storage hybrid power plant, Electric Power Systems Research, 189, 106 631, https://doi.org/10.1016/J.EPSR.2020.106631, 2020a.

Das, K., Philippe Grapperon, A. L. T., Sørensen, P. E., and Hansen, A. D.: Optimal battery operation for revenue maximization of wind-storage hybrid power plant, Electric Power Systems Research, 189, 106 631, https://doi.org/10.1016/j.epsr.2020.106631, 2020b.

Ding, H., Pinson, P., Hu, Z., and Song, Y.: Integrated bidding and operating strategies for wind-storage systems, IEEE Transactions on Sustainable Energy, 7, 163–172, https://doi.org/10.1109/TSTE.2015.2472576, 2016.

DTU HPC Cluster: Sophia HPC Cluster, https://doi.org/10.57940/FAFC-6M81, 2019.

Dykes, K., King, J., DiOrio, N., King, R., Gevorgian, V., Corbus, D., Blair, N., Anderson, K., Stark, G., Turchi, C., et al.: Opportunities for research and development of hybrid power plants, Tech. Rep. TP-5000-75026, National Renewable Energy Lab.(NREL), Golden, CO (United States), 2020.

Fang, Y. and Zhao, S.: Look-ahead bidding strategy for concentrating solar power plants with wind farms, Energy, 203, 117 895, https://doi.org/10.1016/j.energy.2020.117895, 2020.

Fathima, A. H. and Palanisamy, K.: Optimization in microgrids with hybrid energy systems - A review, https://doi.org/10.1016/j.rser.2015.01.059, 2015.

Freire, S. L. M. and Ulrych, T. J.: Application of singular value decomposition to vertical seismic profiling, GEOPHYSICS, 53, 778–785, https://doi.org/10.1190/1.1442513, 1988.

Gene H. Golub, C. V. L.: Matrix computations (3rd ed.), Johns Hopkins University Press, 1996.

Guo, M. and Hesthaven, J. S.: Data-driven reduced order modeling for time-dependent problems, Computer Methods in Applied Mechanics and Engineering, 345, 75–99, https://doi.org/10.1016/j.cma.2018.10.029, 2019.

Han, X. and Hug, G.: A distributionally robust bidding strategy for a wind-storage aggregator, Electric Power Systems Research, 189, 106 745, https://doi.org/10.1016/J.EPSR.2020.106745, 2020.

Hess, M. W., Quaini, A., and Rozza, G.: A data-driven surrogate modeling approach for time-dependent incompressible Navier-Stokes equations with dynamic mode decomposition and manifold interpolation, Advances in Computational Mathematics, 49, 1–27, https://doi.org/10.1007/S10444-023-10016-4/METRICS, 2023.

Hesthaven, J. S. and Ubbiali, S.: Non-intrusive reduced order modeling of nonlinear problems using neural networks, Journal of Computational Physics, 363, 55–78, https://doi.org/10.1016/J.JCP.2018.02.037, 2018.

Hesthaven, J. S., Pagliantini, C., and Rozza, G.: Reduced basis methods for time-dependent problems, Acta Numerica, 31, 265–345, https://doi.org/10.1017/S0962492922000058, 2022.

Huang, X., Wang, J., Huang, T., Peng, H., Song, X., and Cheng, S.: An optimal operation method of cascade hydro-PV-pumped storage generation system based on multi-objective stochastic numerical P systems, Journal of Renewable and Sustainable Energy, 13, 016 301, https://doi.org/10.1063/5.0032455, 2021a.

Huang, X., Wang, J., Huang, T., Peng, H., Song, X., and Cheng, S.: An optimal operation method of cascade hydro-PV-pumped storage generation system based on multi-objective stochastic numerical P systems, Journal of Renewable and Sustainable Energy, 13, 16 301, https://doi.org/10.1063/5.0032455/284873, 2021b.

IBM: IBM® Decision Optimization Modeling for Python (DOcplex), https://github.com/IBMDecisionOptimization/docplex-doc, 2023/09/14, 2023.

Jin, R., Chen, W., and Sudjianto, A.: An efficient algorithm for constructing optimal design of computer experiments, Journal of Statistical Planning and Inference, 134, 268–287, https://doi.org/10.1016/j.jspi.2004.02.014, 2005.

Kanellas, P., Das, K., Gea-Bermudez, J., and Sørensen, P.: Balancing Tool Chain: Balancing and automatic control in North Sea Countries in 2020, 2030 and 2050, DTU Wind Energy E, DTU Wind Energy, Denmark, 2020.

Kingma, D. P. and Ba, J.: Adam: A Method for Stochastic Optimization, https://doi.org/10.48550/arXiv.1412.6980, 2017.

Kitzing, L., Held, A., Gephart, M., Wagner, F., Anatolitis, V., and Klessmann, C.: Contracts-for-difference to support renewable energy technologies – Considerations for design and implementation, European University Institute, https://doi.org/10.2870/379508, 2024.

Koivisto, M., Das, K., Guo, F., Sørensen, P., Nuño, E., Cutululis, N., and Maule, P.: Using time series simulation tools for assessing the effects of variable renewable energy generation on power and energy systems, WIREs Energy and Environment, 8, e329, https://doi.org/10.1002/wene.329, 2019.

Koivisto, M., Gea-Bermúdez, J., and Sørensen, P.: North Sea offshore grid development: combined optimisation of grid and generation investments towards 2050, IET Renewable Power Generation, 14, 1259–1267, https://doi.org/10.1049/iet-rpg.2019.0693, 2020a.

Koivisto, M., Jónsdóttir, G. M., Sørensen, P., Plakas, K., and Cutululis, N.: Combination of meteorological reanalysis data and stochastic simulation for modelling wind generation variability, Renewable Energy, 159, 991–999, https://doi.org/10.1016/j.renene.2020.06.033, 2020b.

Leon, J. P. M., Habbou, H., Friis-Møller, M., Gupta, M., Zhu, R., and Das, K.: HyDesign: A tool for sizing optimization of grid-connected hybrid power plants including wind, solar photovoltaic, and lithium-ion batteries, Wind Energy Science, 9, 759–776, https://doi.org/10.5194/wes-9-759-2024, 2024.

Li, F. F. and Qiu, J.: Multi-objective optimization for integrated hydro–photovoltaic power system, Applied Energy, 167, 377–384, https://doi.org/10.1016/J.APENERGY.2015.09.018, 2016.

Li, L., Jamieson, K., DeSalvo, G., Rostamizadeh, A., and Talwalkar, A.: Hyperband: A Novel Bandit-Based Approach to Hyperparameter Optimization, Journal of Machine Learning Research, 18, 1–52, http://jmlr.org/papers/v18/16-558.html, 2018.

Lian, J., Zhang, Y., Ma, C., Yang, Y., and Chaima, E.: A review on recent sizing methodologies of hybrid renewable energy systems, Energy Conversion and Management, 199, 112 027, https://doi.org/10.1016/j.enconman.2019.112027, 2019.

Lin, C., Liang, H., Pang, A., and Zhong, J.: Data-driven method of solving computationally expensive combined economic/emission dispatch problems in large-scale power systems: an improved kriging-assisted optimization approach, Frontiers in Energy Research, 11, https://doi.org/10.3389/fenrg.2023.1273760, 2023.

Long, Q., Das, K., Pombo, D. V., and Sørensen, P. E.: Hierarchical control architecture of co-located hybrid power plants, International Journal of Electrical Power & Energy Systems, 143, 108 407, https://doi.org/10.1016/j.ijepes.2022.108407, 2022.

Luo, F., Meng, K., Dong, Z. Y., Zheng, Y., Chen, Y., and Wong, K. P.: Coordinated operational planning for wind farm with battery energy storage system, IEEE Transactions on Sustainable Energy, 6, 253–262, https://doi.org/10.1109/TSTE.2014.2367550, 2015.

Murcia Leon, J. P., Koivisto, M. J., Sørensen, P., and Magnant, P.: Power fluctuations in high-installation-density offshore wind fleets, Wind Energy Science, 6, 461–476, https://doi.org/10.5194/wes-6-461-2021, 2021.

Ochoa, T., Gil, E., Angulo, A., and Valle, C.: Multi-agent deep reinforcement learning for efficient multi-timescale bidding of a hybrid power plant in day-ahead and real-time markets, Applied Energy, 317, 119 067, https://doi.org/10.1016/J.APENERGY.2022.119067, 2022.

Pang, A., Liang, H., Lin, C., and Yao, L.: A Surrogate-Assisted Adaptive Bat Algorithm for Large-Scale Economic Dispatch, Energies, 16, https://doi.org/10.3390/en16021011, 2023.

Paska, J., Biczel, P., and Kłos, M.: Hybrid power systems – An effective way of utilising primary energy sources, Renewable Energy, 34, 2414–2421, https://doi.org/10.1016/j.renene.2009.02.018, 2009.

Roy, P., He, J., Zhao, T., and Singh, Y. V.: Recent Advances of Wind-Solar Hybrid Renewable Energy Systems for Power Generation: A Review, IEEE Open Journal of the Industrial Electronics Society, 3, 81–104, https://doi.org/10.1109/OJIES.2022.3144093, 2022.

Shivarama Krishna, K. and Sathish Kumar, K.: A review on hybrid renewable energy systems, https://doi.org/10.1016/j.rser.2015.07.187, 2015.

Stanley, A. P. and King, J.: Optimizing the physical design and layout of a resilient wind, solar, and storage hybrid power plant, Applied Energy, 317, 119 139, https://doi.org/10.1016/J.APENERGY.2022.119139, 2022.

Taha, M. S., Abdeltawab, H. H., and Mohamed, Y. A. R. I.: An online energy management system for a grid-connected hybrid energy source, IEEE Journal of Emerging and Selected Topics in Power Electronics, 6, 2015–2030, https://doi.org/10.1109/JESTPE.2018.2828803, 2018.

Thirunavukkarasu, M., Sawle, Y., and Lala, H.: A comprehensive review on optimization of hybrid renewable energy systems using various optimization techniques, Renewable and Sustainable Energy Reviews, 176, 113 192, https://doi.org/10.1016/j.rser.2023.113192, 2023.

Toubeau, J. F., Bottieau, J., De Greeve, Z., Vallee, F., and Bruninx, K.: Data-Driven Scheduling of Energy Storage in Day-Ahead Energy and Reserve Markets with Probabilistic Guarantees on Real-Time Delivery, IEEE Transactions on Power Systems, 36, 2815–2828, https://doi.org/10.1109/TPWRS.2020.3046710, 2021.

Wiese, F., Bramstoft, R., Koduvere, H., Pizarro Alonso, A., Balyk, O., Kirkerud, J. G., Åsa Grytli Tveten, Bolkesjø, T. F., Münster, M., and Ravn, H.: Balmorel open source energy system model, Energy Strategy Reviews, 20, 26–34, https://doi.org/10.1016/j.esr.2018.01.003, 2018.

Xu, B., Oudalov, A., Ulbig, A., Andersson, G., and Kirschen, D. S.: Modeling of Lithium-Ion Battery Degradation for Cell Life Assessment, IEEE Transactions on Smart Grid, 9, 1131–1140, https://doi.org/10.1109/TSG.2016.2578950, 2018.

Yang, Y., Guo, S., Liu, D., Li, R., and Chu, Y.: Operation optimization strategy for wind-concentrated solar power hybrid power generation system, Energy Conversion and Management, 160, 243–250, https://doi.org/10.1016/J.ENCONMAN.2018.01.040, 2018.

Zhang, G., Hu, W., Cao, D., Liu, W., Huang, R., Huang, Q., Chen, Z., and Blaabjerg, F.: Data-driven optimal energy management for a wind-solar-diesel-battery-reverse osmosis hybrid energy system using a deep reinforcement learning approach, Energy Conversion and Management, 227, 113 608, https://doi.org/10.1016/j.enconman.2020.113608, 2021.

Zhang, X., Yuan, Y., Hua, L., Cao, Y., and Qian, K.: On Generation Schedule Tracking of Wind Farms With Battery Energy Storage Systems, IEEE Transactions on Sustainable Energy, 8, 341–353, https://doi.org/10.1109/TSTE.2016.2598823, 2017.

Zhang, X., Gu, J., Yuan, Y., Hua, L., and Shen, Y.: Scheduling wind-battery energy storage hybrid systems in time-of-use pricing schemes, IET Generation, Transmission & Distribution, 12, 4435–4442, https://doi.org/10.1049/IET-GTD.2017.1878, 2018.

Zhu, L.-P., Yin, X., and Zhu, L.-X.: Dimension Reduction via an Alternating Inverse Regression, Journal of Computational and Graphical Statistics, http://www.jstor.org/stable/25765379, 2010.

Zhu, R., Das, K., Sørensen, P. E., and Hansen, A. D.: Optimal Participation of Co-located Wind-battery Plants in Sequential Electricity Markets, TechRxiv. Preprint, https://doi.org/10.36227/techrxiv.21618984.v1, 2022.

Zhu, R., Das, K., Sørensen, P. E., and Hansen, A. D.: Enhancing profits of hybrid wind-battery plants in spot and balancing markets using data-driven two-level optimization, International Journal of Electrical Power and Energy Systems, 159, 110 029, https://doi.org/10.1016/j.ijepes.2024.110029, 2024.